Magnetic Resonance Studies on Maple Sap

by

Michael Gill

B.Sc. UNB 2007; M.A. Acadia University 2010

A Thesis Submitted in Partial Fulfillment
of the Requirements for the Degree of

Master of Science

in the Graduate Academic Unit of Physics

Supervisor: Benedict Newling, PhD, Department of Physics

Examining Board: Abdelhaq Hamza, PhD, Department of Physics, Chair

Igor Mastikhin, PhD, Department of Physics

John Kershaw, PhD, Department of Forestry and Environmental Management

This thesis is accepted by the Dean of Graduate Studies

THE UNIVERSITY OF NEW BRUNSWICK

July, 2024

Abstract

Maple syrup is an important product to the Canadian economy and to our broader national identity. The sugar concentration of maple sap plays a vital role in the overall profitability of syrup producers. Currently one must damage a tree to extract sap to determine its sugar concentration, and as such, the sap from very young trees cannot be tested. The work of this thesis lays the foundations for non-invasive testing of sugar concentration of maple sap using magnetic resonance. Beginning with extruded sap, magnetic resonance measurements are proposed and assessed then implemented on real sap filled maple wood using portable, handheld sensors within the lab setting. Improvements for the procedures and instrument designs are also discussed.

Dedication

I would like to dedicate this work to the memory of my father, who passed away during the completion of this work. Even though he is gone, in the quiet moments of the day, I can still hear his voice asking what I intend to do after I graduate.

Acknowledgements

This work would have been abandoned long ago if not for the kindness and support of my supervisor Dr. Benedict Newling and my wife Alison Gill. Their unwavering belief carried me during those times when I didn't believe in myself. Thank you.

Table of Contents

List of Tables

List of Figures

Chapter 1

Introduction and background material

1.1 General Introduction to this thesis

Motivation

The seeds of the research presented in this thesis were planted years ago on a cool spring day as I tended a roaring fire for the backyard production of maple syrup. Upwards of 6 hours of boiling time goes into each litre of finished syrup so there is ample time for mindful reflection and pondering. It was while sitting in the snow, watching the orange flames dance across the pot that I first asked myself "How does the sugar affect the maple sap's magnetic resonance (MR) signal and would that be useful and worthwhile information to research?"

Goals of current work

Looking back, the MR effects of sugar in solution were well understood and published (Aroulmoji et al., 2012). However, maple sap is much more than a simple solution of sugar and water. Reducing sap to such a simple model severely underestimates the challenges of interpreting MR measurements on natural sap and performing measurements in situ.

Of course, sucrose is the compound of interest for both syrup hobbyists like myself and the commercial syrup industry, which in Canada has annual exports in excess of 500 million CAD. More informed formulations of that original campfire pondering would be "how does one peer through the chemical cocktail in maple sap using MR to isolate the effect of the sucrose? How does the structure of wood impact such a measurement? What are some of the relevant applications of these techniques to the broader maple industry?"

Overview of included research

This thesis is the culmination of years of study and research and contains two articles that seek to answer the above questions. Chapter 2, which was published in *Sugar Tech*, is principally concerned with time-domain MR on extruded maple sap, comparing its signal lifetime to that of simple sugar water. In this chapter molecular self-diffusion of water is identified as the target quantity to measure in order to isolate the effects of the sucrose from those of the other constituents. This chapter, then, answers the question of how MR can assess sucrose concentration without interference from other chemical constituents in solution. Chapter 3, which has been submitted to *Wood Science and Technology*, demonstrates how such a diffusion measurement can be performed on maple wood with a portable MR sensor in an attempt to develop a method to measure the sugar concentration within a maple treeling without damaging its bark and sap vessels. Much of this chapter is dedicated to a discussion on how to best overcome challenges related to conducting MR measurements on woody structure. The third chapter also includes recommendations for future hardware to refine and improve such a measurement, and an assessment of what value such a measurement could have to the maple industry.

While these chapters are standalone articles and contain some important background information, a lot of material is still assumed. The remainder of the current chapter provides a deeper exploration of the foundations of magnetic resonance and of the physiology and processes important to maple trees and their sap. Also a review of other MR studies and applications to wood science is included in order to give wider scholarly context to the original research of this thesis.

1.2 MR Background

What is Magnetic Resonance

The following is an overview of some key principles of magnetic resonance, that serve as a basis for the research contained in chapters 2 and 3 of this thesis, and generally relies on the structure and treatment in Nishimura (2016). When supplemental material is needed, explicit references are given. Full derivations from first principles are omitted for the sake of brevity, and instead key results alone are highlighted.

Magnetic resonance (MR), sometimes referred to as nuclear magnetic resonance (NMR), is a powerful, non-invasive measurement technique that utilizes an external magnetic field ($\mathbf{B}_0$) to condition a sample. The field is then altered with a burst of radio-frequency energy and the sample's response is measured through an induction coil. The resulting signal is digitized and can be analyzed to provide important and relevant information about the sample. At its most fundamental, MR is a quantum mechanical phenomenon, since the sample response happens on an individual nuclear level and arrises from the quantum property spin. However, owing to the correspondence principle, which states that the predictions of quantum theory must correspond to classical physics in the limit of very large systems of quanta, MR can be treated classically, as will be the case in the following discussion (Eisberg and Resnick, 1985).

MR-active Nuclei

Not all nuclei are suitable for MR. For the work done in this thesis, ^{1}H is the only nucleus of interest. However, any nucleus with an odd number of protons and/or neutrons is subject to magnetic resonance because they possess spin angular momentum, which gives rise to two separate, yet equally important, responses when the nucleus is exposed to an external magnetic field, $\mathbf{B_0}$. For simplicity, nuclei possessing spin angular momentum are referred to as spins.

The first effect to be considered is Zeeman splitting: the separation of two degenerate energy levels by the presence of a magnetic field. After the degeneracy has been lifted and the spins are given time enough time to equilibrate in accordance to T_1 (defined below), the spins' associated magnetic moment will be aligned either parallel or anti-parallel to $\mathbf{B_0}$. Once this process of magnetic polarization is complete, the sample will possess a net magnetization ($\mathbf{M_0}$) determined by the difference between the populations. The majority of the magnetic moments will align parallel to the external field as this is the lower energy state, which then defines the direction of $\mathbf{M_0}$. By convention, the direction of $\mathbf{B_0}$ defines the z-axis (or *longitudinal* axis). The magnitude of $\mathbf{M_0}$ can be calculated by means of a Boltzmann distribution, and is given by

$$M_0 = \frac{N\gamma^2\hbar^2 I(I+1)B_0}{3kT},$$

where N is the number of spins, I is the quantum number, ħ is Plank's constant, k is the Boltzmann constant, and T is the temperature of the sample.

The second effect vital to MR is precession. Associated with spin angular momentum is the magnetic moment **μ**, which experiences a torque when placed in an external magnetic field. In turn, the applied torque causes the magnetic moment to precess about $\mathbf{B_0}$, like a gyroscope in a gravitational field, at the Larmor frequency, given by the Larmor equation $\omega = \gamma B_0$ where γ is the gyromagnetic ratio specific to the nuclei under investigation.

There are then two distinct frames of reference for describing MR behaviours: the frame rotating at the Larmor frequency and the stationary (or laboratory) frame. Certain effects are more naturally described in one frame versus the other, and I will use both frames in the description that follows (Callaghan, 2011).

Signal and the RF Pulse

Once an ensemble of MR-sensitive nuclei are conditioned by the $\mathbf{B_0}$ field, a useable output (signal) is created by applying a radio-frequency (RF) pulse tuned to the Larmor frequency. This RF pulse generates a secondary magnetic field, $\mathbf{B_1}$, perpendicular to $\mathbf{B_0}$, which causes the precessing ensemble magnetization to rotate into the transverse (xy) plane. While in the transverse plane, the continued precession of the ensemble magnetization induces a current in a nearby pickup coil, and that current is digitized as the MR signal.

The power and duration of the RF pulse can be adjusted to control how much the net magnetization of the sample is rotated away from the z-axis. A 90° pulse represents full rotation into the transverse plane, while a 180° pulse yields a full inversion of the spin populations changing $\mathbf{M_0}$ into -$\mathbf{M_0}$. There are MR techniques that employ pulses besides 90° and 180°, however these two were the only pulse angles used in the current work.

Time Evolution and Signal Lifetimes

The time evolution of sample magnetization in a uniform $\mathbf{B_0}$ field is described phenomenologically by the Bloch equation:

$$\frac{d\mathbf{M}}{dt} = \mathbf{M} \times \gamma \mathbf{B_0} - \frac{M_x \mathbf{i} + M_y \mathbf{j}}{T_2} - \frac{(M_z - M_0)\mathbf{k}}{T_1}.$$

Separating the Bloch equation into its longitudinal (M_z) and transverse (M_{xy}) components yields two fundamental differential equations, which govern many MR experiments.

$$\frac{dM_z}{dt} = \frac{M_z - M_0}{T_1}$$

$$\frac{dM_{xy}}{dt} = -\frac{M_{xy}}{T_2}$$

The solutions to these equations are exponential functions with the characteristic time constants T_1 and T_2. They are referred to as the longitudinal relaxation and transverse relaxation time constants, for obvious reasons, but also as the spin-lattice and spin-spin time constants respectively.

Spin-lattice (T_1) relaxation is best described conceptually in terms of energy level splitting. The input of RF energy at the Larmor frequency depopulates the low energy level to the advantage of the higher energy level. Spin-lattice relaxation characterizes the sample's return to the lowest energy configuration, i.e. the return to thermal equilibrium.

Spin-spin (T_2) relaxation is caused by energy exchange between the spins of a sample, and is simplest both mathematically and conceptually when treated in the rotating frame because that frame of reference features a stationary M_{xy} when on resonance (Callaghan, 2011). On the microscopic level, a broadening of resonant frequencies results from the interactions between the z-component of one spin's magnetic dipole with that of its neighbouring spins. Thus, the total field experienced by certain spins is either weaker or stronger than B_0. The spins at the higher field precess more rapidly than those at the lower field. The macroscopic consequence is the introduction of a phase difference between precessing magnetizations, thus the transverse magnetization is lost as spins fall out of phase with one another.

T_1 and T_2 relaxation are connected by means of the Larmor frequency ω and the correlation time τ_c, which in a liquid is a time associated most strongly with the local Brownian motion. This connection was investigated in a hugely influential 1948 paper by Bloembergen, Purcell, and Pound. In it, the authors develop a theory to explain and offer predictions for relaxation behaviour that has since come to be known as BPP theory. The idealized BPP theory assumes isotropic molecular motion, but its trends are quite representative even in more complicated cases. In general, for short correlation times, T_1 and T_2 are similar. As correlation time increases, T_1 has a field dependant

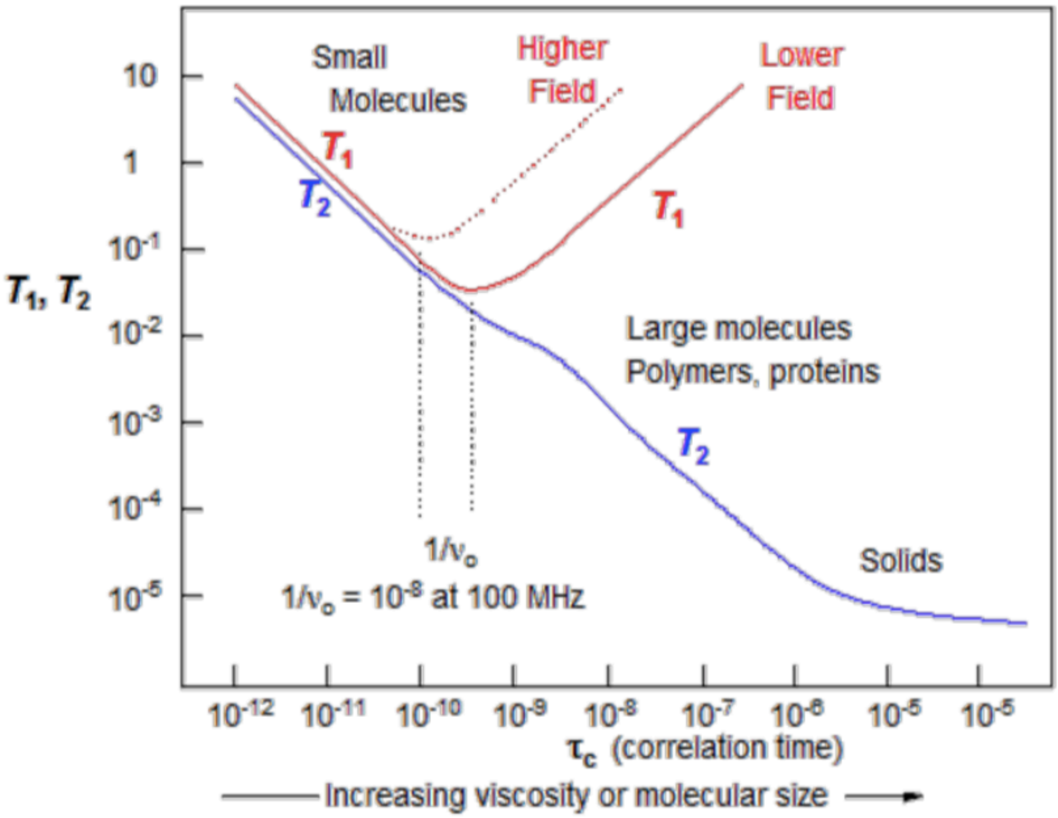

Figure 1.1: Graphical representation of BPP model. Credit: Bruce Balcom, MRI course notes 2019, after Bloembergen et al. 1948.

minimum whereas T_2 decreases monotonically. BPP theory is often visualized graphically for ease of use (Figure 1.1).

As previously stated, the output in an MR experiment is not magnetization directly, but rather the digitized signal, S(t). The observed signal is directly proportional to sample magnetization, $S_0 \propto M_0$, and since the units of signal are arbitrary, we are able to convert the solutions to the separated Bloch equation into signal equations (see section below).

Pulse sequences and signal equations

The formation of a signal echo, illustrated in Figure 1.2, is vital to many applications of and measurements with MR. While there are many types of echos based on how they are formed (e.g. stimulated from three consecutive pulses or by a gradient), the one most important to this thesis is the spin echo. In order to form a spin echo, magnetization is tipped into the transverse plane by a 90° RF pulse (Figure 1.2A). Spins are then allowed some time τ to evolve during which they fall out of phase (Figure 1.2B). Some of this dephrasing is homogeneous, resulting from small (ppm) inhomogeneities in $\mathbf{B_0}$, and can be refocused to form the spin echo. Then a 180° RF pulse is applied which flips the transverse magnetization, inverting the phases (Figure 1.2C), and the spins come back into phase after time τ following the second pulse (Figure 1.2D).

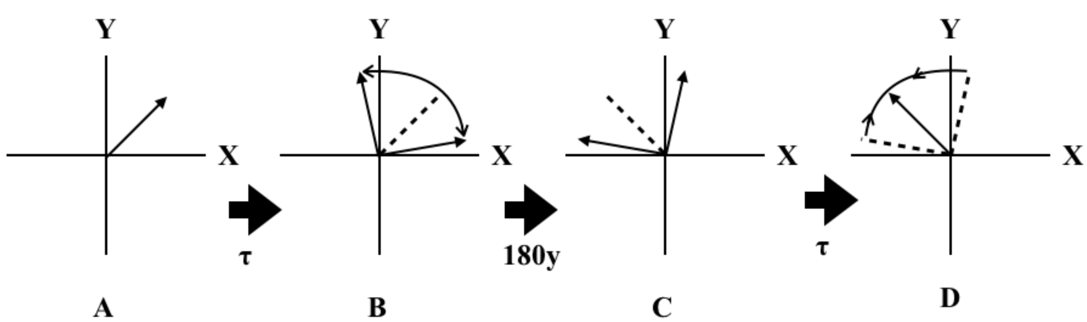

Figure 1.2: Formation of a spin echo. A) Magnetization is tipped into the xy-plane. B) During time τ spins dephase. C) Following a 180y pulse, spins are rotated. D) After time τ spins run back into phase.

MR experiments consist of a pulse, or series of pulses, which manipulate sample magnetization before the signal is detected and digitized. There is a multitude of well established pulse sequences for a host of applications. The research that follows relies on only four separate sequences: inversion recovery; saturation recovery; Carr-Purcell-Meiboom-Gill echo train (CPMG); and Pulsed Gradient Spin Echo (PGSE).

T_1 is an important experimental parameter in MR. In order to ensure consecutive measurements are mutually independent, the sample must be allowed to return to thermal equilibrium, which requires waiting $5 \times T_1$. The T_1 relaxation time constant is routinely measured using either an inversion recovery or a saturation recovery pulse sequence.

For an inversion recovery (IR) sequence, magnetization is first inverted by a 180° RF pulse, then allowed some time *t* to recover, at which point, magnetization is tipped into the transverse plane then digitized. This process is repeated with different *t*s to build a recovery curve. The signal equation for this procedure, deriving from the solution to the longitudinal portion of the Bloch equation with initial magnetization set to $-M_z$ is $S(t) = S_0(1 - 2e^{-\frac{t}{T_1}})$.

Saturation recovery (SR) is similar to the inversion recovery sequence with one major difference. Instead of inverting the sample magnetization with an 180° RF pulse, the sample is preconditioned with RF energy to ensure the measurement begins with no longitudinal magnetization. The saturation scheme used in the current work was to subject the sample to a series of unevenly spaced 90° pulses which annihilates any residual magnetization from previous experiments, thus net magnetization at t = 0 is 0. As such the signal equation is $S(t) = S_0(1 - e^{-\frac{t}{T_1}})$. Using SR in lieu of IR is primarily done when either T_1 is really long (on the order of tens of seconds to minutes, as is the case with solids) or when it is difficult to invert sample magnetization, as is the case when working in an inhomogeneous field (see below).

The CPMG sequence creates a spin echo (described above) then continually brings the spins back into phase through successive 180y RF pulses, typically separated by the same time as between the original 90x-180y pair that formed the initial echo.

$$90x - \tau - (180y - \tau - \text{echo} - \tau)_n$$

Each time the spins are brought back into phase, the amplitude of the echo decreases, reflective of the loss of phase coherence due to spin-spin interactions (T_2). The signal equation for the CPMG sequence is $S(t) = S_0 e^{-\frac{t}{T_2}}$. The relative phases, indicated by the x and y above, of the initial and refocusing pulses is an important (and defining) feature of the CPMG sequence. Since programming and implementing precise and exact pulse lengths is nearly impossible, small pulse length errors will occur in the sequence resulting in incomplete rephasing. Even a small error of 1° to 3° will have a huge impact on the acquired signal as these errors are additive with each applied pulse. By adding the relative phase difference between the 90 and 180 pulses, the CPMG sequence reduces the effect of these inevitable pulse errors.

The Pulsed Gradient Spin-Echo sequence, as its name indicates, employs magnetic field gradients in addition to the spin-echo. Two gradients of equal duration and magnitude are inserted one after each of the 90x and 180y RF pulses in the spin echo sequence. Following the 90x pulse, spins will accumulate additional phase dispersion due to the presence of the gradient. When an attempt is made to bring them brought back into phase by the 180 pulse, only spins that have remained stationary since the first pulse will be completely in phase (Figure 1.3). If the pulse timings are held constant, the gradient strength can be adjusted to provide more or less spin dephasing. If there is a distribution of displacements in the sample, then the stronger the gradient the more signal loss due to irreversible dephasing. Thus by repeating the experiment with progressively stronger gradient values, the incoherent motion (molecular self-diffusion) of a sample can be effectively measured (Callaghan, 2011) or the distribution of velocities in the sample can be measured (Selby, 2023).

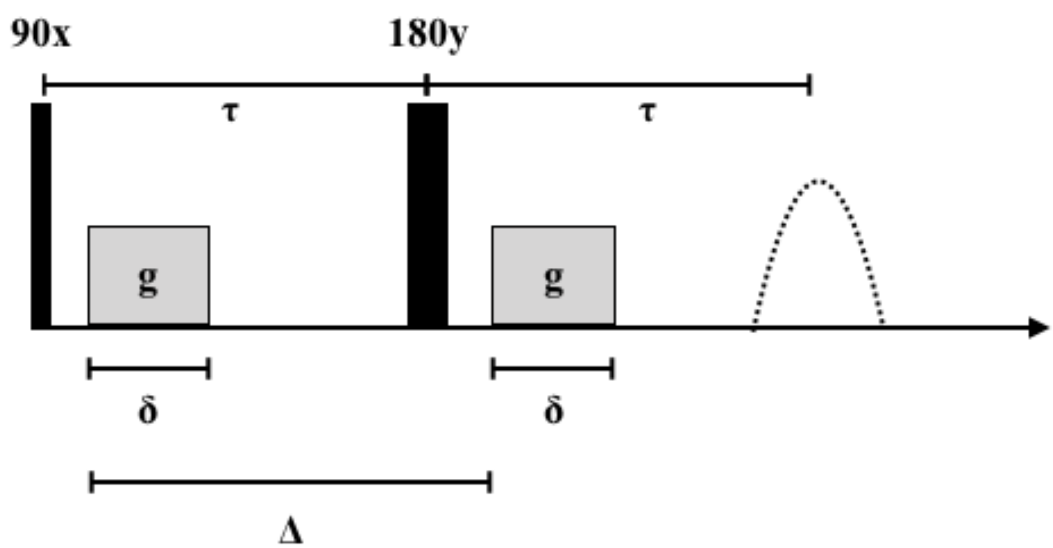

Figure 1.3: Diagram of the PGSE pulse sequence. The magnetic field gradients are characterized by the time parameters δ and Δ and by magnitude g.

Excitation in an Inhomogeneous Field

The above description of MR pulses and sequences assumes the sample is immersed in a nearly homogeneous B_0 field (this was the condition for the experiments detailed in chapter 2). When the main field is inhomogeneous, either by way of the natural inhomogeneity of many portable MR sensors constructed from permanent magnets (as was the case for chapter 3 of this work) or due to the application of a steady gradient, the dynamics of RF excitation and sample relaxation require additional consideration. For the discussion below, I will be assuming a magnetic field with a well defined, centrally peaked shape that falls away at the edges (e.g. a Gaussian distribution in three dimensions or a rounded boxcar).

When conditioned in an inhomogeneous magnetic field, the sample will have a distribution of resonance frequencies. Some portion of the sample will resonate at the main frequency while the remainder will have various frequency offsets. The RF pulse itself naturally excites a grouping of frequencies due to the bandwidth of the pulse, $\Delta\nu$, being equal to the inverse of the RF pulse duration. The excited group of spins have positions determined by

$$\Delta\nu = \frac{1}{t_{pulse}},$$

$$\Delta\nu = \frac{\gamma}{2\pi}\mathbf{G}\cdot\mathbf{r},$$

where **G** describes the spatial distribution of field inhomogeneity (which is in effect a field gradient), and **r** is the displacement vector centred at **G** = **0**. Since the location and amount of sample excited by the RF pulse becomes a feature of the pulse duration in an inhomogeneous field, all pulses used in a sequence must have the same duration. Only the pulse power can be adjusted to create a 90 or 180° pulse, for example.

In multi-echo sequences, such as a CPMG, an echo will form from spins rephasing due a combination of effects from the field inhomogeneities and the multiple pulses. These create a set of echoes that overlap the CPMG echo train beginning with the second echo (Casanova and Perlo, 2011). For the purpose of converting CPMG data into value(s) (or distributions) of T_2, the first echo is disregarded. Also, the T_2 measured in an inhomogeneous field will represent a mixture of spin-spin relaxation, spin-lattice relaxation, and diffusive attenuation as phase is lost due to the incoherent motion of spins within the effective gradient (Casanova and Perlo, 2011). As such, the measured T_2 is often called the effective T_2, T_{2eff}. More will be said about the relationship between T_2 and T_{2eff} in chapter 3. Therefore, handheld, naturally inhomogeneous MR sensors have the advantage of being able to conduct measurements of molecular self-diffusion without the need for bulky and expensive gradient coils and gradient amplifiers, making them a sensible choice for the type of measurements we will encounter in chapter 3 of this thesis.

Any precise MR measurement of diffusion requires a complete knowledge of the magnitude of the gradient or effective gradient that is responsible for enabling the diffusive attenuation of the signal. In a completely homogeneous sample, the strength of the gradient solely depends on the instrument itself so using a calibration sample for a diffusion measurement is feasible. However, when a sample has regions of materials that possess greatly different magnetic susceptibilities, such as pockets of air or clusters of metals, quantifying the gradient experienced by the sample is much more complicated. As magnetic field lines pass from one material to another, they distort, creating additional field gradients internal to the sample (Griffith, 2017). This effect, known as a magnetic susceptibility mismatch, is well known and very pronounced in rocks. The strength of these internal gradients scale with B_0. These effects can be avoided by orienting the sample in such a way that the B_0 field does not cross the boundaries of material with differing susceptibilities or by reducing the B_0 field strength until they no longer impact the results of the experiment (Callaghan, 1991). While internal gradients driven by susceptibility differences in woody structure are small (Terenzi et al., 2013), they can have a very large impact when they are comparable to the magnitude of the effective gradient used to measure diffusion, as we shall see in chapter 3.

MR signal within porous media

When magnetic spins are confined in a sufficiently small pore, edge effects become an important consideration when interpreting the MR signal. Spins in contact with a wall have limited mobility and are considered bound in contrast to free water in the interior of a pore. Bound water will have a much reduced signal lifetime compared to free water. Spins in these two environments exchange, and within the fast exchange limit, the total signal detected from a pore will be a weighted average between the free and bound water. The smaller the confinement the quicker the relaxation due to wall effects beginning to dominate the weighted average of relaxations. More will be said on this in the third chapter including the effect on the signal equation.

1.3 Maple background: tree structure and sap

In the early days of this research project, a wood scientist, whose brain I was picking, remarked that the differences between hardwood and softwood trees were night and day. This may be true from a certain, specialized perspective, but MR is largely insensitive to these differences. To a MR spectrometer, wood is little more than a collection of protons bouncing around set of regularly shaped, unconnected chambers.[1] Without the use of highly specialized MR techniques like cryoporometry (see below), MR is insensitive to the nano-scale structures in wood. As for tree characteristics like growth rate and crown and root development, these hardly matter for a snapshot measurement of the wood structure and its contents.

There are, of course, important differences to the shape and distributions of pores (cells or vessels) between families and genera of trees. Many MR studies of wood are motivated by industry concerns, thus they focus on tree species important for lumber and logging. Therefore, I will begin by offering a comparison of woody (xylem) structure between maple trees and coniferous trees commonly used for timber. Then, I will proceed to a discussion of aspects of maple tree sap important to the syrup industry: composition; transport mechanisms; and environmental factors in sap production.

Xylem structure in various tree species

Woody plants are divided into two groups: angiosperms and gymnosperms. Gymnosperms are typically evergreen trees with needle leaves including fir, spruce, and pine varieties which are most commonly used for lumber. Maple trees belong to the angiosperm group. In both groups, sap transport is conducted through young xylem, but the character of the xylem varies between the groups.

---

[1] This statement is overly simplistic and is made purposely in contrast to the preceding sentence. The reality, as far as the research contained in these pages is concerned, falls somewhere between the two points of view and will be elaborated on in short order.

In gymnosperms, xylem cells form tracheids which are of similar dimensions and rays which are oriented radially to the tree stem. Seasonally, tracheids that form early in the year have thinner walls and wider cross-sections than late year growth, therefore there is a marked change in wood density throughout the year. Visually, this annual variation gives rise to tree rings (Figure 1.4).

Figure 1.4: Tree xylem under 200x magnification: maple (right), fir (left) showing seasonal variation of tracheid size (growth ring). Sap flow would be out of page. Photo credit: Michael Gill.

Angiosperms are further subdivided into ring-porous and diffuse-porous trees, with maple trees being one of the diffuse-porous varieties. Angiosperm xylem contains both tracheids like gymnosperms and much larger vessels which act as the primary sap conduits (Figure 1.4) as well as fibres which do not conduct sap. Unlike gymnosperms, cell wall thickness and vessel width in diffuse-porous trees does not vary throughout the season, meaning that the distribution of pore sizes is much more narrowly peaked in maple trees compared to spruce trees, for example. This trait becomes very important in chapter three as it a permits the treatment and interpretation of relaxation data to deduce values of water self-diffusion.

Relevant Aspects of Maple Sap

The physical process of sap exudation in maple trees is not completely known and remains a matter of some debate (Perkins, 2009). The leading hypothesis combines factors such as the freeze-thaw cycle of water xylem during periods of flow, water phase transitions caused by varying internal pressures, and osmotic barriers to sucrose migration between types of xylem cells (Tyree, 1983). Mathematical modelling has also shown that the depression of the freezing point by dissolved sucrose plays an important role in the internal pressures required for sap flow (Graf et al., 2015).

Environmental and soil conditions play a role in determining the sugar concentration and sap flow prior to the maple season in late winter and early spring although the variation due to these factors is less than that of tree specific characteristics (Rademacher et al., 2023). The abundance of nitrogen in the soil has been shown to correspond to higher sugar concentrations in sap (Wild and Yanai, 2015). This is not a surprising finding when one considers the role nitrogen has in supporting photosynthesis. Maple trees have a very shallow root mass with 70 to 80% of roots occurring at 20cm below the surface, making them sensitive to freezing stress (Robitaille et al., 1995). During the winter months, colder temperatures and deeper snowpack tend to increase spring sap flow (Harrison et al., 2020). The snowpack also affects the sugar concentration in at least two ways. It has an insulating effect on the soil, roots, and lower stem holding them near 0°C, which is the optimal temperature for starch hydrolysis (Cortes and Sinclair, 1985; Decker et al., 2003). In addition, when the snowpack is shallow or absent entirely, the soil becomes more acidic, which decreases the availability of nitrogen that in turn reduces the tree's ability to produce carbohydrates due to the role nitrogen plays in supporting photosynthesis (Decker et al., 2003).

As mentioned above, maple sap is a water solution of sugars (primarily sucrose), at least twelve inorganic metals and minerals, seven organic acids, and ten phenolic compounds. Detailed lists of the sap constituents can be found in Perkins and van den Berg 2009 and Legace et al. 2015. In the present work, MR signal was produced by ^1H meaning the metals and minerals could not directly produce signal. However, the effect of ferromagnetic and paramagnetic metals, such as manganese, copper, and iron, on MR signal is non-trivial and will play a key role in interpreting the data in succeeding chapters. While the organic components of maple sap contain hydrogen, they are in such low concentrations that their presence is not detectable in low resolution MR scanners.

1.4 MR on Trees and Woody Structure

Woody structure and the water contained therein has a long history of being the subject of MR studies. While there have been many changes in the field since the early wood studies of the late 1980s and early 1990s, e.g. hardware and types of samples studied, the kernel of the experiments has remained largely unchanged — T_2 measurements.

In 1987, Menon et al. demonstrated, using a variety of cedar (a gymnosperm), that the T_2 of a woody sample was separable into the sample's two primary water environments: within the cell wall and inside the cell cavity. Monitoring the signal intensity of these water populations yields information about the dynamics of wetting and drying that is unavailable through other experimental means (Lamason et al., 2015). In 1992, Araujo et al. refined the MR treatment of wood by noting that since T_2 is a function of pore size, and that the pore size of tracheids exist as a distribution, then the T_2 ought to be treated as a continuous distribution. It should be noted that Araujo et al. illustrated this point with another gymnosperm (white spruce).

While this refinement is undoubtedly true, many MR studies of wood elect to treat T_2 as a discrete quantity rather than as a distribution. The choice between these two approaches is likely dictated by what property of the wood is of interest. Measurements of total moisture content have been used to track important dynamics within woody structure without the more complex distribution analysis. For example, Windt and Blümler, 2014, using their portable NMR CUFF magnet design, were able to directly relate increases to bulk water in an oak stem to diameter stem growth (the tree uptakes additional water immediately before cell division) and demonstrated that this measurement was more sensitive than a conventional pressure dendrometer. In addition, Lamason et al. 2017 were able to monitor the emptying of large vessels through successive bulk T_2 measurements resolved to two discrete time constants, as saturated wood logs were dried to below the fibre saturation point.

When more detailed information about the porous structure of wood is required, experimenters rely on a distribution analysis through use of an inverse Laplace transform (ILT).[2] The vegetative elements of trees contain a far greater diversity of cell types and sizes than the woody structure so those studies often require the use of T_2 distributions (Sorin et al., 2018). Also, knowing how various wood treatments affect porosity is important industry information, which is readily available through an ILT of relaxation data for both pulped wood (Foston and Ragauskas, 2010) and intact wood (Elder et al., 2006).

An interesting alternative method for probing the pore sizes of wood is cryoporometry. Taking advantage of the lowered freezing point of tightly bound water, cryoporometry measures the MR signal of frozen wood which is then correlated to a pore size. This method is successful because only liquid phase water is readily detectable by MR (ice has an incredibly short T_2 which requires special attention to detect). Freezing point suppression occurs in pores on the scale of nanometers, which makes cryoporometry an attractive method for investigation the finer woody structure as opposed to the vessels chiefly responsible for sap flow (Gao et al., 2015; Cao et al., 2021).

Over the last two decades, several groups have made much headway in developing MR sensors that are suitable for deployment in fields and greenhouses for in situ plant and tree measurements. While the term "portable" is often bandied about, the weight of these sensors is often not negligible. Many of these sensors also come

[2] The name "inverse Laplace transform" is an unfortunate misnomer although it is cemented in the MR vocabulary. The function itself uses a Fredholm integral of the first kind as its kernel. Imbedded in the ILT algorithm is a regularization parameter, α, which has the effect of smearing or sharpening the data. Extreme caution needs to be used when choosing α to ensure the resulting analysis is physically representative of the sample. As such, one needs to have a good reference and some prior knowledge of the sample's physical nature to avoid misinterpretations.

equipped with gradient coils for density and flow imaging, which can reduce instrument portability.

A truly unique in situ sensor was used for long term drought response monitoring in aspen trees. It featured an electromagnet made from 41cm diameter Helmholtz coils producing a static B_0 of 860μT (for comparison the Earth's field is ~50μT, while low-field bench top MR instruments operate at a strength of 100s of mT). At such an ultra-low field and without gradients, imaging and flow experiments are impossible, and even simple relaxation experiments are impractical. However, this sensor was capable of a single pulse detection of signal (free induction decay), which enabled the gathering of information about the changes of bulk water within the tree stem (Malone et al., 2016).

A very large, outdoor MR system was assembled by a Japanese group. The magnet offers a 200mT field over a gap of 160mm, more than enough for a young but established tree. The tradeoff, of course is the weight. The permanent magnets alone weigh 520kg (Nagata et al., 2016). Complete with imaging gradients, this system was able to spatially resolve sap flow within a living tree and measure the differences in flow rate of early, late, and new xylem growth (Terada et al., 2019).

The final in situ sensor considered here belongs to a Dutch group. The sensor is a C-shaped, permanent magnet design operating at 242mT and weighing 4.5kg with an air gap of 30mm (Windt et al., 2021). Originally, this probe head was tested using bulk, time-domain measurements. It was later incorporated into an full, portable imaging system, capable of similar measurements described above only on much smaller specimens (Meixner et al., 2021).

The original work of this thesis differs from what comes before in two key regards. Firstly, our concern is not the location or structure in which the tree sap (water) resides, but rather we are interested in one aspect of its chemical composition: sucrose concentration. We use knowledge of sap vessels in maple wood in combination with MR data to infer chemical information. Secondly, we do so on a novel group of MR sensors that have naturally inhomogeneous magnetic fields, which permit diffusion and flow measurements without the need for a set of external gradients and gradient amplifiers.

Chapter 2

The determination of sucrose content in maple sap using time-domain magnetic resonance[3]

2.1 Abstract

The natural variation of sucrose concentration in maple tree sap is investigated using time-domain magnetic resonance (MR). The current study, which includes a concise introduction to the relevant MR properties, is a demonstration of principle showing how the relaxation time constant T_2 and the self-diffusion coefficient relate to the amount of sucrose and ionic content present in the collected sap samples. T_2 and self-diffusion coefficient for maple saps from six different trees, each sampled weekly in the spring of 2019, were measured using MR. The results were plotted against the sucrose concentration of each sample with the aim of determining if either quantity could serve as the basis for a non-invasive sucrose measurement for maple trees. The T_2 relaxation time constant was found not to be a reliable proxy for sucrose content in maple sap as it showed sensitivity to the slight changes in sap chemistry throughout the season and natural variation from tree to tree. The diffusion coefficient, determined through a standard pulsed-gradient spin-echo (PGSE) experiment, was insensitive to the changes in sap chemistry, and showed a strong relationship to sucrose content. A diffusion measurement is thus proposed as the most suitable candidate for a non-invasive sucrose measurement for maple tree sap.

---

[3] This chapter has been published by *Sugar Tech* on Feb 14, 2022. Permission to reproduce this work has been granted under licence number 5754351464627

2.2 Introduction

The production of maple syrup and related confections is an important industry in Eastern Canada with total production in 2019 having a value of over $500 million CAD (Government of Canada, 2020). The processing of maple sap into maple syrup, in which water is removed from sap through reverse osmosis and boiling to bring the overall sugar content from ~2% (pure sap) to ~64% (commercial syrup), is time and energy intensive. Within this process, any increase in efficiency can have a very significant impact on profitability. The combination of high production costs and a premium finished product means that the maple industry is prone to intentional mislabelling and counterfeiting. Differentiating between genuine and fake syrup is an important component of the enforcement of industry standards (Clément et al., 2014).

Maple sap is a solution that ranges in sugar concentration from 1% to 5% and water content from 95% to 99%. Variations of sugar content depend on the tree, environmental conditions during growth, and time of year, with sucrose making up between 96%-99% of the total sugars in pure sap (Perkins & van den Berg, 2009). Complete analysis of sap chemistry identifies seasonal variation of sugars and other dissolved solids such as minerals and phenolic compounds, all in trace amounts (Lagacé et al., 2015).

While the total sugar content in tree sap varies due to external conditions, the relative sweetness of one tree with respect to its neighbouring trees has been shown to be consistent; a sweet tree is always a sweet tree (Taylor, 1956). An obvious potential avenue to improve the efficiency of the syrup process is to collect sap only from the sweetest trees, and if possible, identify and encourage the sweetest maple trees in the growth stage of a maple stand.

The standard approach to testing the sweetness of sap relies on refractometry. The sapwood is punctured, allowing for the extraction of a sample to be tested in a refractometer. Because this process requires some damage to the tree, there is a lower limit to the age and size of trees that can withstand the stress of the procedure. For the collection of large amounts of sap in the case of syrup production, only trees of at least 25cm diameter at breast height are tapped (Perkins & van den Berg, 2009). In order to collect small volumes of sap from smaller trees for testing, a process called micro-tapping was developed. However, this newer procedure is still invasive and is only rarely implemented in trees 3 years of age with a stem diameter of 1 to 2 cm. Micro-tap testing is usually done once trees are 5 to 7 years old (Staats, 1992).

The benefit of early sugar testing of saplings extends beyond the commercial sugarbush. There have been a number of large progeny studies, with an experimental timescale of forty years, the goal of which was to research the possibility of producing a sweeter nurse stock of maple trees through select breeding. Due to pests, weather, and human activity many of these trees did not survive long enough to be tested, limiting the reliability of the eventual study results (Staats, 1992). A completely non-invasive sugar test that could be implemented in the youngest of saplings would be a powerful new tool in these and other types of studies.

The continued development of low-cost and portable magnetic resonance (MR) sensors opens a new horizon of measurements that can be used to study and understand industrial and agricultural production (Capitani et al., 2017; Blümich et al., 2009). As yet, the authors are unaware of any peer-reviewed studies of the MR properties of maple sap; however, there have been numerous studies on other sucrose solutions, and the aim of this paper is to differentiate the MR behaviour of natural maple sap from that of a pure sucrose solution and to describe a reliable method for assessing sucrose content of sap using MR.

2.3 MR Background

Unlike MR Spectroscopy, which has a line width resolution to distinguish each hydrogen environment in a given molecule, the resolution of typical time-domain MR equipment is insufficient to characterize a molecule based on its chemical shift, as demonstrated in Figure 2.1. In lieu of directly observing the spectrum, time-domain MR monitors the decay of signal following one or more radio frequency (RF) pulses.

There are two fundamental lifetimes in MR: the spin-lattice relaxation time (T_1), which describes a sample's return to thermal equilibrium; and the spin-spin relaxation time (T_2), which describes the loss of signal due to dephasing of neighbouring "spins" (^1H nuclei in the present measurements). Since loss of signal can also stem from the Brownian motion of molecules within the sample itself, time domain MR also provides a means to measure molecular self-diffusion, typically reported as a diffusion coefficient (D).

The time interval between successive measurements, commonly referred to as either the last delay (LD) or the repetition time (TR), needs to be sufficiently long to allow the sample to return to thermal equilibrium to ensure no residual magnetization is carried over ensuring each measurement yields an independent result. The standard LD is equal to $5 \times T_1$ of the sample.

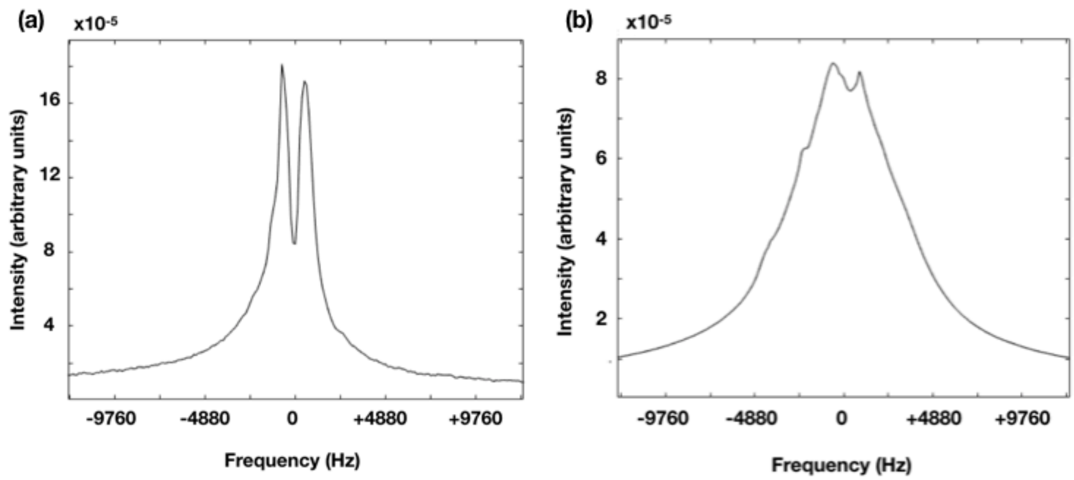

Fig. 2.1 Fourier Spectra taken on a 100-MHz superconducting MR scanner. The vertical axes are not comparable. The two spectra represent solutions of different concentrations and different sized vials. (a) Sucrose-D_2O solution: the two, low resolution peaks correspond to the backbone hydrogen on the sucrose molecule and the OH groups. (b) Sucrose-H_2O solution: the spectral peaks relating directly to the sucrose molecule, as seen in 1(a) are dwarfed by the bulk water peak.

When paramagnetic ions, such as Cu^{2+} and Mn^{2+}, are in solution, the presence of multiple varying local magnetic fields causes a shortening of both characteristic times T_1 and T_2 of a solution due to more rapid dephasing of magnetic spins (T_2 effect) and an increase in the relaxation efficiency of nearby water protons due to long-range electron relaxation of the paramagnetic ions (T_1 effect) (De León−Rodríguez, et al., 2015). These effects increase linearly with respect to the inverse of T_1 and T_2 with increasing concentration of paramagnetic ions (Parigi and Luchinat, 2018). Since diffusion is the process of random molecular motion, it is unaffected by the presence of paramagnetic ions.

At relatively low concentrations of sucrose, the MR signal is dominated by water, as can be seen in the Fourier spectrum in Figure 2.1b, and as such the sample will have a single T_2 value (compared to mixtures such as oil and water, which have two or more measured T_2 values). But by virtue of the sucrose being dissolved, the water neighbouring the sucrose molecule will form a hydration shell or layer, often referred to as "bound water", the population of which will be directly proportional to the concentration of sucrose. Thus the measured T_2 will be a weighted average of that of the free water and the bound water and is described by the following equation:

$$\frac{1}{T_{2obs}} = \frac{a}{T_{2free}} + \frac{b}{T_{2bound}},$$

where *a* and *b* are the concentrations of free water and bound water respectively. Since *a* and *b* must sum to 1, we can rewrite the equation as

$$\frac{1}{T_{2obs}} = \frac{1}{T_{2free}} - \frac{b}{T_{2free}} + \frac{b}{T_{2bound}}.$$

Finally, noting that the concentration of bound water is much much less than 1, we can approximate the second term by zero, which yields a expression connecting the inverse of our observed T_2 and the concentration of sucrose

$$\frac{1}{T_{2obs}} = \frac{1}{T_{2bound}} \cdot b + \frac{1}{T_{2free}}.$$

Previous MR experiments involving sucrose solutions have all reported this linear relationship (Aroulmoji et al., 2012; Fabri et al., 2005; Ziegler et al., 2002; Eustace & Jordan, 1995).

2.4 Material and Methods

Sap was collected from six maple trees in rural New Brunswick (Canada) for four consecutive weeks during March 2019 and kept frozen after initial measurements. The March 11th samples were spoiled due to a freezer malfunction before the diffusion coefficients could be measured; however, those samples were viable during the relaxation phase of the experiment. At the time of spoilage, only the March 11th samples were in the freezer; the remaining samples were kept in a chemical fridge and were unaffected as a result.

Samples were collected at each tree by manually transferring sap from buckets, which had been emptied the previous day after sap flow had ceased, into unused plastic sample vials. This was to ensure sap tested was entirely the product of a single day's run. Sucrose was measured in the field at point of collection and again in lab before storage. All six trees were sampled at each of the four time points and a second stem of one tree was sampled beginning in week two for a total of 27 individual samples.

The mineral content of the non-spoiled sap samples was determined by ICP/ES with the assistance of the UNB Civil Engineering waste water testing lab using a Varian Vista MPX Axial ICP ES (Inductively Coupled Plasma Emission Spectrometer) instrument. Detected wavelengths (nm) were as follows: Ca (396.847); Cu (327.395);

Fe(259.940); K (769.897); Mg (280.270); Mn (294.921); Na (589.592); P (214.914); and Zn (206.200). Testing for Ca, K, Mg required a twentyfold dilution with distilled water, whereas the remaining elements were determined with unadulterated sap.

Sucrose content is given in Brix percent (%Bx) as measured by a Hanna Instruments portable, digital refractometer, HI 96801 (Woonsocket, RI) with a resolution of 0.1%Bx and precision of ±0.2%Bx.

The diffusion and relaxation experiments were conducted on a Nalorac (Martinez, CA) 2.4 T 32 cm i.d. horizontal bore superconducting magnet with a water-cooled 7.5 cm Nalorac gradient set driven by Techron (Elkhart, IN) 8710 amplifiers. The RF probe was a homemade 4.5 cm i.d. birdcage probe driven by a 2 kW Tomco (TomcoTechnologies, Stepney, Australia) RF amplifier. The console was a Tecmag (Houston, TX) Redstone.

Spin-spin (T_2) lifetimes were measured using the Carr-Purcell-Meiboom-Gill (CPMG) sequence with an echo time of 1 ms and 90° and 180° RF pulse durations of 15 μs and 30 μs respectively. While not included in our the results, the spin-lattice (T_1) relaxation rate was measured using a standard inversion recovery (IR) pulse sequence using the same pulse RF pulse lengths already noted (Callaghan, 2011). Each T_2 measurement took approximately 2 minutes.

The gradient strength in the diffusion measurements was calibrated against distilled water at 14°C using 1.7156 x 10^{-9} m^2/s for the value of the diffusion coefficient, as calculated by the equation given in Holz et al., 2000. These measurements were done using a standard pulsed gradient spin-echo (PGSE) sequence (Callaghan, 2011). The maximum gradient strength was 0.278 T/m with $\Delta = 30$ ms and $\delta = 4$ ms, and the overall measurement time was approximately 7 minutes.

Temperature control was achieved by resting samples in a cool air stream generated from nitrogen boil-off controlled with an Omega (Omega Engineering, Stamford, CT) 6002 temperature controller that was stable to ±0.5°C. Sample temperature was measured before and after measurement using a standard immersible alcohol thermometer with range of -20°C to 110°C with precision of ±0.5°C.

Horizontal error bars in Figure 2.3 reflect the precision of the refractometer while the vertical error bars show the standard deviation of multiple measurements of the diffusion coefficient.

In addition, low-field relaxation experiments were conducted on a 10 MHz Bruker Minispec MQ10 NMR Analyzer (Rheinstetten, Germany) using the CPMG sequence with an echo time of 10 ms and 90° and 180° RF pulse duration of 2.08 μs and 4.38 μs.

2.5 Results

Two types of artificial saps were made by diluting pure sucrose, produced by Sigma-Aldrich, and commercially available maple sugar, produced by Acadia Maple in Nova Scotia, in distilled water to achieve a representative concentration of 1%-5% sucrose. The sucrose concentration of an actual sap sample, was also varied with distilled water as an additional point of comparison. Figure 2.2 illustrates the relationship between relaxation lifetime and sucrose concentration. If the sucrose in the solutions were primarily responsible for affecting spin-spin relaxation, then each solution would have similar T_2 values. As can be seen in Figure 2.2, however, this was not the case. The maple solutions relaxed faster than pure sucrose. Other solutions (for example a second source of maple sugar) gave additional results consistent with Figure 2.2.

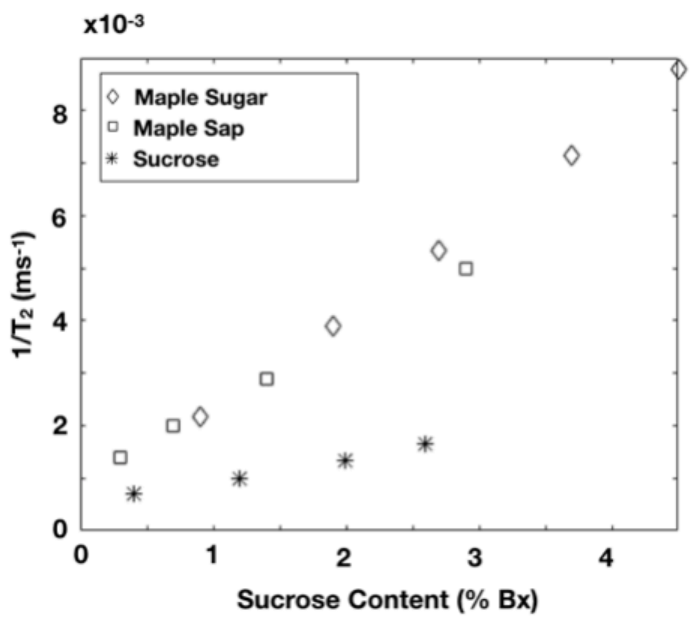

Fig. 2.2 T_2 relaxation plotted against sucrose content (measured with a refractometer) for three types of sugar solutions. Note that the sap is diluted with distilled water, which gives rise to a $1/T_2$ that varies linearly with increasing sucrose content, consistent with pure sucrose solutions.

Because chemical composition of sap is known to vary both from tree to tree and over time, saps from six maple trees were collected over four weeks in March 2019. The T_2 relaxation of these saps was measured and plotted against their measured sugar content. Again, if the variation of sucrose between samples was the principal cause of relaxation differences, the plot of relaxation versus sucrose content would produce a linear plot, regardless of other natural variations in sap chemistry. The scatter seen in

Figures 2.3a and 2.3b demonstrates relaxation behaviour that is attributable to something other than just sucrose and that this variability is not affected by the field strength of the MR scanner. The T_1 relaxation of these samples was also measured and showed similar scatter as that in Figure 2.3.

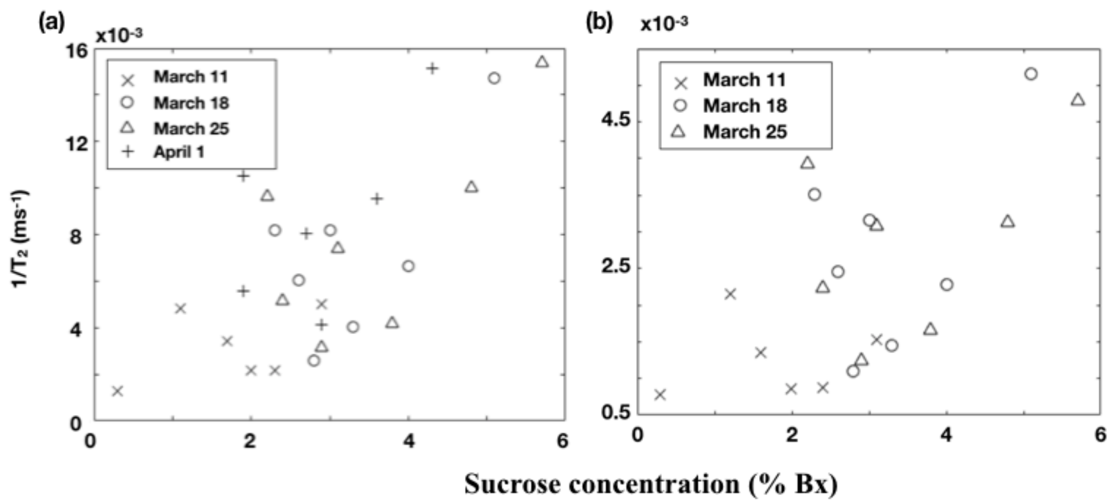

Fig. 2.3 T_2 relaxation plotted against sucrose content for maple sap taken from six different trees sampled over a four week period in the spring of 2019. Beginning in the second trial week, a second tap was added to a multistem tree to yielding an additional data point. Measurements taken at (a) 100 MHz and (b) 10 MHz. A mechanical breakdown in the 10 MHz instrument delayed the measurement of the final set of sap samples, and the instrument was decommissioned before measurements could be completed.

Table 2.1 shows the mineral analysis results, which were consistent with previously published reports of maple sap content (Perkins & van den Berg, 2009, and Lagacé et al., 2015). Cu and Fe were detected weakly at concentrations near to and below the detection limit of the instrument. Cu is included in Table 2.1 because it was at detectable concentration levels in all but five samples, whereas Fe is excluded because it appeared at the detection limit in only five of the twenty samples. Owing to its strong magnetic properties, it is important to mention within the context of a MR study.

Table 2.1 — Summary of mineral content in tested sap

Element	Average (mg/L)	Minimum (mg/L)	Maximum (mg/L)	Standard Deviation (mg/L)
Ca	16.49	2.81	44.39	12.30
Cu	0.020	nd	0.032	0.007
K	85.80	25.16	204.53	48.10
Mn	2.81	0.32	9.05	2.21
Mg	3.00	0.49	11.29	2.61
Na	1.69	0.46	4.65	1.29
P	5.70	1.53	14.23	3.85
Zn	0.202	0.045	0.871	0.199

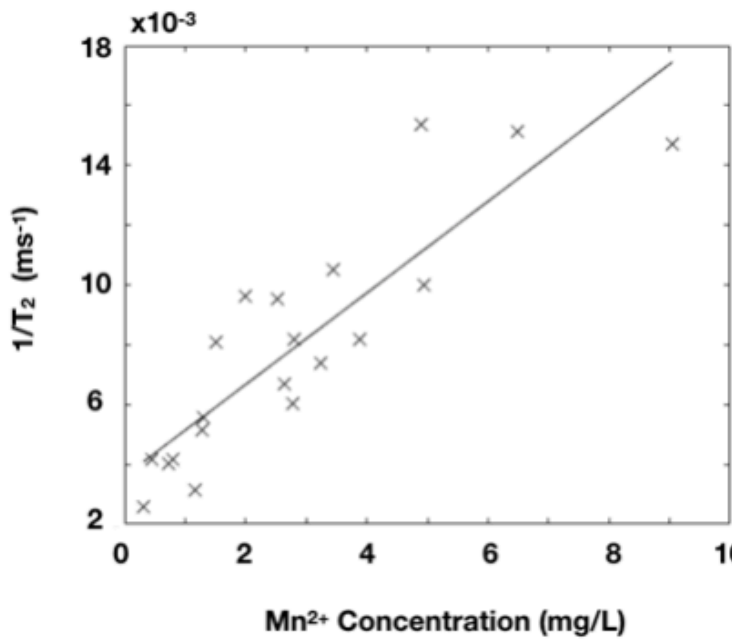

Fig. 2.4 T_2 relaxation plotted against manganese content for maple sap for all sap samples that remained unspoiled at the time of ICP/ES analysis. Line of best fit has an R-squared value of 0.7667.

Since Mn^{2+} is both an effective relaxation agent and is found in significant, highly variable concentrations in maple sap, both in the literature and in the current study, the measured spin-spin relaxation of the sap samples is plotted against their manganese concentration (Figure 2.4). The plot shows a convincingly linear relationship between manganese concentration and the inverse of T_2 with an R-squared value of 0.7667.

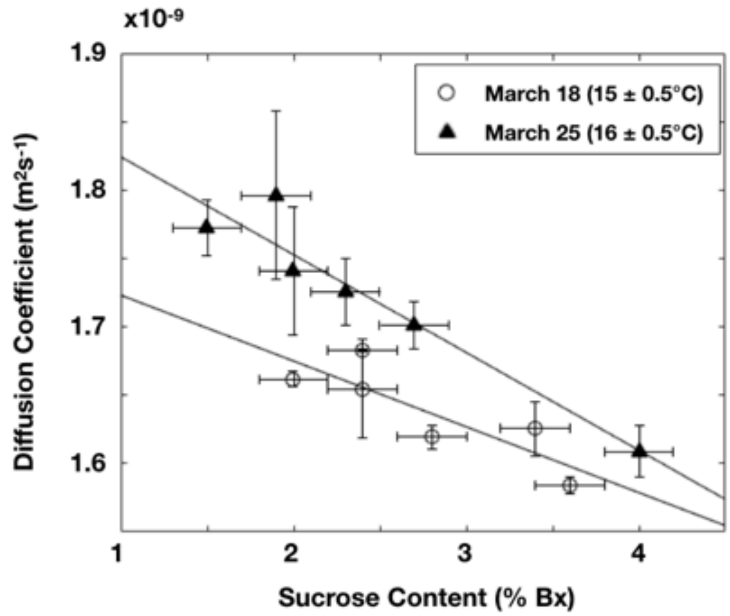

Fig. 2.5 Plot of the molecular self-diffusion coefficient of water in maple saps versus measured sucrose content. The volume of sap collected from the multistem tap was insufficient for all measurements and did not survive into the diffusion trials. The COVID-19 pandemic delayed testing of the fourth set of saps, then the 100MHz magnet suffered a fatal quench before testing could be concluded. Sap samples used for the diffusion measurements were poured off from the partially thawed main samples used in previous experiments resulting in slightly different sucrose contents being reported between figures 2.3 and 2.5. R-squared values of the fit lines on the March 18 and March 25 data points were 0.7219 and 0.9194 respectively.

Next the water diffusion coefficients of the viable sap samples were measured. The March 18 and March 25 saps were measured on separate days during the summer of 2019 during which the ambient temperature of the lab varied substantially. Even with careful temperature control, we were unable to conduct both sets of measurements at the same temperature; however, each measurement within both sets were the same within the precision of the thermometer. Temperature control was necessary because molecular self diffusion is highly sensitive to temperature (Holz et al., 2000). In fact, the measured change in diffusion coefficient from a 1% increase in sucrose concentration was less than the change brought about by a 1°C increase in temperature as seen in Figure 2.5. Despite this issue in the relative sensitivity to temperature and sucrose concentration, Figure 2.5 shows that self-diffusion of maple saps is dependent upon the sucrose concentration and not upon other changes in sap chemistry.

A previous study of the diffusion coefficient of water in sucrose solution identified an apparent exponential relationship (Aroulmoji et al., 2012); however, that study investigated a much larger range of sucrose concentrations (~5.1% to ~44.5%, as read from their published figure). Since any exponential function is approximately linear at points near zero, we have chosen a straight-line fit for the current data. The March 25th set shows a stronger linear relationship than that from March 18th, as evidenced by their R-squared values of 0.9194 and 0.7219 respectively. It is not entirely surprising that the set with the smallest range of concentrations would yield a fit with the most uncertainty. In addition to the statistical quantity of R-squared, the reasonableness of a linear fit comes from the extrapolated diffusion value of the 0% concentration point (the y-intercept), which should be the diffusion coefficient of water at the given temperature. In this case, both fit lines produce water diffusion values that are within the uncertainty range of calculated values: $1.772\times10^{-9}m^2/s$ (fit) to $1.765 \pm 0.181\times10^{-9}$ m^2/s (calculated) for March 18, and $1.897 \times 10^{-9} m^2/s$ (fit) to $1.8152 \pm 0.184 \times 10^{-9} m^2/s$ (calculated) for March 25.

2.6 Discussion

When taken alongside the apparent linear relationship between Mn^{2+} and measured relaxation (Figure 2.4), the non-linearity in Figures 2.3a and 2.3b clearly demonstrate that any relaxation measurement of maple sap will only communicate information about paramagnetic concentrations present within the sap. The R-squared value of 0.7667 in Figure 2.4 indicates that while manganese dominates the relaxation behaviour in maple sap, T_2 is still being effected by other paramagnetic ions and molecules. Even though the scope of the current study is limited in its sample size, large sap chemistry studies confirm that the variation seen in this study is typical (Lagacé et al., 2015). Therefore, one can reasonably expect that any attempt to correlate sucrose concentration to basic relaxation in maple sap to be impossible without first having a detailed knowledge of the full chemistry of the particular sap sample. This observation could be exploited to form a useful measurement for the detection of fake/counterfeit maple syrup.

Since the relaxation times of maple saps were highly sensitive to the natural variation of paramagnetic ions, the measurement of T_2 could provide a quick and simple way to differentiate pure maple syrup from artificial syrups. As sap is transformed into syrup, a substance called “niter” or “sugar sand” forms and falls out of solution. The composition of this precipitant is highly variable and does contain small amounts of copper and manganese (Perkins & van den Berg, 2009). The fact that some manganese survives this process can be inferred from Figure 2.2, which shows that diluted maple sugar (a maple product made by continued heating of pure syrup) has a comparable relaxation curve as maple sap, both being distinct from a simple sucrose solution. A standard Brix measurement and a value for the T_2 of the syrup in question would be enough to locate it on either a sucrose calibration curve for artificial syrups or within a typical range of genuine maple syrup.

The water self-diffusion coefficient is not affected by the presence of paramagnetic ions, and so the seemingly linear lines of best fit in Figure 2.5 are not unexpected. Since the concentration of all dissolved solids in sap pale in comparison to sucrose, the molecular motion of H_2O is most affected by the increased viscosity caused by the dissolved sucrose. Because the mineral composition and sucrose content of the saps tested in the current study were representative of general maple sap, the observed trend in Figure 2.5 ought to be generalizable as well. In order to more fully define the functional relationship between diffusion coefficient and sucrose concentration in maple sap, other more extensive studies will need to be conducted with a broader range of sucrose contents and across a larger variation of experimental temperatures — an endeavour far beyond the scope and limited sample size of the current study.

Any attempt at exploring and mapping the relationship between sucrose and diffusion in maple sap will need to deal with the extreme temperature dependence of the diffusion process. The temperature control and monitoring in the current study was limited to 0.5°C. Owing to the wide range of sucrose content present in the saps tested, particularly the March 18th set, the correlation between sucrose and diffusion was not overshadowed by the coarse temperature control.

The time required to measure a sample's diffusion coefficient is largely constrained by two factors: the number of gradient values used and the LD of the sequence. In our measurements, 11 different gradient values were used to provide the highest confidence in our reported values. In practice, however, fitting of the data was excellent and the measurement could have been performed with fewer gradient steps. By following the method of Stait-Gardner, 2008, the diffusion measurement can occur at the steady state magnetization instead of waiting for the return to thermal equilibrium after each iteration. The added measurement speed becomes a tradeoff with overall accuracy of the measurement, however with care, a suitable balance can be found. By implementing the aforementioned changes, this 7 minute measurement could be accomplished in as little as 2 minutes.

A planned follow-up study will see sets of cuttings of young coppice wood (diameter less than 5mm) tested using a portable MR device in order to confirm that changes in self-diffusion can be observed in plant cuttings. The study will employ a permanent magnet sensor with a constant gradient (Ross et al., 2021) which will simplify the measurement of diffusion by eliminating the need to have well controlled and defined magnetic field gradients.

2.7 Conclusion

Two magnetic resonance measurements were performed on extruded vials of maple sap to determine how the MR signal relates to the sucrose concentration of maple sap. The spin-spin relaxation time constant, T_2, was heavily influenced by the natural variations in paramagnetic ions in the sap and those effects dominated over the effect of sucrose concentration. The results shown in Figure 2.1 imply that the presence of paramagnetic ions, particularly manganese, in sap could be exploited allowing the differentiation between real and artificial maple syrup using T_2. The diffusion coefficient of maple sap was found to decrease as sucrose concentration increased, meaning that diffusion could be used as a proxy for sucrose given a well defined calibration curve built upon further clinical trials. Since MR is, by nature, non-invasive, these findings can be developed into non-invasive/non-destructive measurements of sugar content potentially benefiting the maple industry at both the forest planning and product fidelity levels.

Chapter 3

Magnetic resonance diffusion measurements of sap within maple wood pores and their relationship to sucrose concentration

3.1 Abstract

The sucrose concentration of maple sap is closely related to the molecular self-diffusion of the sap water. The diffusion coefficient was measured for sap within the large pores of maple wood using two newly designed portable magnetic resonance (MR) sensors. The diffusion coefficient was then plotted against the sucrose content of the sap, measured traditionally using a refractometer, after it had been extruded from the maple sticks at the time of harvest. Physically sensible diffusion coefficients were produced and several experimental, instrumentation, and physical properties important to this measurement are discussed. A new set of instrument characteristics are proposed to better facilitate more sensitive diffusion measurements in the future.

3.2 Introduction

The sucrose content of maple sap is an important factor for the production of maple syrup and related confections. The higher the sucrose concentration, the less time and energy is required for syrup production. The typical maple stand will yield sap with 2% sucrose on average, but on an individual basis, maple trees can yield sap ranging from 0.5% to 6% sucrose (Taylor, 1956). Seasonal and environmental influences are partly responsible for this range, but a genetic component is arguably more important (Perkins and van den Berg, 2009).

Based on this hypothesis, the ability to test and screen young trees for high sugar output could be transformational for the industry. Doubling the average sweetness of a newly planted maple stand, thereby greatly increasing the efficiency of the syrup process (Weaver et al., 2020), would be advantageous. As the Earth evolves under the effects of climate change, the areas suitable for harvesting maple sap are forecast to move northward over the next 50 to 100 years, meaning now is the optimal time to begin the process of cultivating the most efficient maple stands (Pelletier, 2023).

Gill and Newling (2022) demonstrated that magnetic resonance (MR) measurements of diffusion coefficients of extruded maple sap can be correlated to the concentration of sugar within the sap. The current paper investigates the application of that idea to sap contained within the woody structure. As a proof of concept, we show how a diffusion measurement can be implemented on a limited number of tree cuttings with portable, permanent magnet sensors, outline the assumptions and best practices that simplify the data analysis, and propose a set of custom properties that will be used to build a new sensor in order to improve the reliability and applicability of this measurement.

3.3 MR Background

Our analysis relies on the surface relaxation model of porous media and the diffusion sensitivity of MR methods, both of which are covered in great detail in *Translational Dynamics & Magnetic Resonance* (Callaghan, 2011). Immediately applicable portions are outlined below.

When placed in an external magnetic field, MR sensitive nuclei precess at a frequency given by the Larmor equation (eq. 3.1), which relates the strength of the external field, B_0, and gyromagnetic ratio of the nucleus, γ, to the frequency, ν. In practice, field strength is often expressed as the frequency of precession in megahertz (MHz) rather than an absolute value in tesla (T).

$$\nu = \frac{\gamma B_0}{2\pi} \text{ [eq. 3.1]}$$

The Proteus and clamshell sensors utilized in this study are constructed from two identical permanent magnets in a sandwich orientation with samples loaded between them. This orientation provides a constant, inhomogeneous magnetic field (B_0) in which time-domain measurements are performed (Ross et al., 2021; Morin et al., 2024).

Time-domain MR measures the signal lifetime after the application of one or more radio frequency (RF) pulses. The two fundamental MR lifetimes are determined by T_1 and T_2. The first describes a sample's return to thermal equilibrium following excitation by an RF pulse. The second describes the loss of observable MR signal amplitude due to a variety of molecular processes. Since there is a constant gradient in the magnetic field, measurements of the T_2 time constant will yield signal attenuation determined by both interactions between nuclei (the typical T_2 relaxation mechanism, termed spin-spin) and molecular self-diffusion. This apparent T_2 is reported as T_{2eff} and it is related to the sample's intrinsic (spin-spin) T_2 according to eq. 3.2.

$$\frac{1}{T_{2_{eff}}} = \frac{1}{T_2} + \frac{D\gamma^2 G^2 (TE)^2}{12} \text{ [eq. 3.2]},$$

where D is the diffusion coefficient of the sample, γ is the gyromagnetic ratio of hydrogen, G is the effective gradient experienced by the sample, and TE is echo time, an experimental variable that is the sampling interval in the Carr-Purcell-Meiboom-Gill (CPMG) pulse sequence.

The majority of MR signal from wood arises from the MR-active ^1H nuclei in the hydrogen atoms of water. The cellular structure of the wood determines the unique water environments which will generate MR signal. There are three main environments that are detectable by these types of MR measurements in pore-diffuse wood such as maple: cell wall water; small pore water; and, large pore water. When water molecules are in contact with a surface, their mobility is reduced thereby shortening the spin-spin lifetime. Molecules within the middle of a confined space undergo rapid exchange with their neighbouring molecules along the walls yielding a weighted average spin-spin lifetime. As a confinement's size decreases, the relative population of short lifetime spins increases making these wall effects more pronounced. The smaller the cavity, the shorter the average T_2.

Directly comparing reported T_2 values for these three environments in the literature is not straightforward as the strength of the B_0 field also impacts relaxation. In general, however, a T_2 less than 1 ms is associated with cell wall water, in the range of 1 to 10 ms is associated with water in small pores, while greater than 10 ms is considered large pore water. (Da-Yan et al., 2012; Gao et al., 2015; Lamason et al., 2017)

Since there is a distribution of pore sizes within the category of large/small pores and T_2 is sensitive to pore size, attributing a single T_2 value to a set of pores is a simplification. In reality a distribution of pore sizes ought to return a similar distribution of T_2 values (Araujo et al., 1992). Wood, however, provides such a sharply peaked distribution that the simplification is justified, as seen in the T_2 distribution in Figure 3.1.

Owing to the effect of pore size on spin-spin relaxation, a term needs to be added to eq. 3.2. Eq. 3.3 describes how T_{2app} relates to T_2 for porous media within an inhomogeneous magnetic field.

$$\frac{1}{T_{2app}} = \frac{1}{T_2} + \rho_2 \frac{S}{V} + \frac{D\gamma^2 G^2 (TE)^2}{12} \text{ [eq. 3.3],}$$

where ρ_2 is the surface relaxivity and S/V is the surface area to volume ratio of the pore. Note that the first two terms of this equation are constant for a given sample within a static magnetic field at constant temperature.

The signal to noise ratio (SNR) is an important characteristic of MR at low fields. SNR is defined as the ratio of the signal at its highest point divided by the standard deviation of the noise when no signal is detected (eq. 3.4).

$$SNR = \frac{S_{max}}{\sigma_{noise}} \text{ [eq. 3.4]}$$

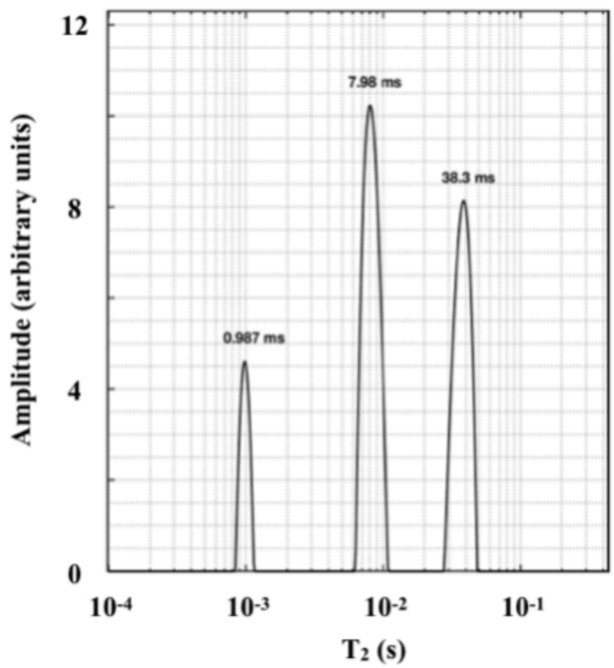

Fig. 3.1 T_2 distribution of a maple cutting measured at 20 MHz with an echo time of 0.6 ms. The three peaks correspond to water in (from left to right) cell walls, small pores, and large pores with their values in agreement with published literature.

3.4 Materials and Methods

Woody samples were collected in March 2022. The end of the wood was cut and bent to allow sap to run into a glass vial for optical testing. Once sufficient sap was extracted, the stem was severed at a length of approximately 32 cm. Stem diameters ranged from 6 mm to 6.7 mm. The ends were immediately sealed with a commercial grade marine epoxy to slow moisture loss. Samples were stored in a freezer once the epoxy set. Samples were given 1 hour to thaw and equilibrate to lab temperature prior to MR measurements. Interestingly, measurements done on samples directly from the freezer had a similar amount of total signal compared to those which had time to acclimatize to the ambient lab temperature, indicating that the sap in the wood pores remained in the liquid phase even at temperatures well below 0°C, which agrees with the observations of Ishikawa et al. (2009).

MR measurements were conducted with two homemade, portable, low field (less than 1 T) MR sensors, which could be deployed in a greenhouse or other non-lab setting. These sensors were powered by a 2 kW Tomco RF amplifier (TomcoTechnologies, Stepney, Australia) with a Tecmag Redstone console (Houston, TX). The first sensor was a 20 MHz Proteus magnet, constructed from two permanent disc magnets with an effective gradient of 57 G/cm and a 2.9 cm by 0.9 cm rectangular solenoid RF probe. The second was a 1.7 MHz clamshell magnet with pitched, rectangular ceramic magnets, having a 1.8 cm diameter cylindrical solenoid RF coil with a 20 G/cm effective gradient.

At 20 MHz, T_{2app} lifetimes were measured using the CPMG sequence with echo times (TEs) ranging from 1.5 ms to 2.4 ms and an RF pulse duration of 4.8 μs. Each CPMG measurement required 512 averages with 500 ms between each average. One T_{2app} measurement required 7.5 minutes. To calculate a diffusion value, T_{2app} was measured at 4 different TEs for a total measurement time of 30 minutes.

At 1.7 MHz, T_{2app} lifetimes were measured using the CPMG sequence with TEs ranging from 2.5 ms to 5.5 ms and an RF pulse duration of 1.44 μs. Each CPMG measurement involved taking 2400 averages with 150 ms between each average. One completed measurement of T_{2app} took approximately 20 minutes. To calculate a diffusion value, T_{2app} was measured at 4 incremental TEs for a total measurement time of 80 minutes.

Sucrose content is given in Brix percent (% Bx) as measured by a Hanna Instruments portable, digital refractometer, HI 96801 (Woonsocket, RI) with a resolution of 0.1% Bx and precision of ±0.2% Bx.

With TEs greater than 0.8 ms, signal from the cell walls is not readily detectable, so our T_{2app} will have two components: a short component relating to the small pores (~3.5 μm diameter) and a long component relating to the large pores (~50 μm diameter). On the time scale of the measurement, the effective diffusion coefficient of water trapped in the small pores is small enough that it is neglected in the analysis. In contrast, the large pores are large enough that most diffusing water molecules do not encounter the pore wall, so the effective diffusion coefficient is reduced by the pore confinement compared to free water, but not greatly reduced. Therefore, the diffusion coefficient is calculated only for the large pores by using the long lifetime component of T_{2app}. Our measurements indicated roughly a 30% reduction in diffusion coefficients compared to those of extruded sap reported previously (Gill and Newling, 2022).

In order to fit the acquisition data at 20 MHz, the short component of T_{2app} was fixed at its value as measured at the shortest TE for each set of acquisitions. Since the following analysis depends only upon how the diffusive attenuation changes the observed spin-spin relaxation, and since the short component is not expected to be affected by diffusion, this choice is justified. Equation 3.5 gives the root mean square displacement for molecules under Brownian motion with D being the unrestricted diffusion coefficient and t being the time during which molecules are free to move, which in the present case is TE.

$$\langle |\vec{r}\,| \rangle = \sqrt{2Dt} \text{ [Eq. 3.5]}$$

Representative numbers from the 20 MHz study demonstrates that the apparent diffusion coefficient for water molecules confined to $\langle |\vec{r}\,| \rangle = 3.5$ μm is so small that no diffusive attenuation of the MR signal is to be expected (Eq. 3.3). In the 1.7 MHz measurements, the longer choices of TE effectively eliminated the signal from the small pores leading to a simplified data analysis.

Calculation of the diffusion coefficient was done by first measuring the long component of T_{2app} with different TEs, then plotting $(T_{2app,\ long})^{-1}$ against TE^2. As described in eq. 3.3, the resulting figure yields a straight line plot whose slope is $D\gamma^2G^2/12$. Because $\gamma^2G^2/12$ is common between all samples, the slope can be used as a proxy for D to facilitate a quick comparison between samples.

Molecular self-diffusion is highly temperature sensitive (Holtz, 2000). All measurements were done without external temperature control, instead relying on stability of lab temperature, which was steady at 26 ± 0.5°C for the 20 MHz measurements. The lab temperature during the 1.7 MHz measurements was less steady, ranging from 25°C to 28°C. Measured stem diffusion coefficients are normalised (below) with respect to the calculated diffusion coefficient of free water at ambient temperature, in order to remove any temperature effect.

3.5 Results

Nine twigs out of eleven were chosen for analysis in this study in order to minimize variation in diameter while maximizing the range of sap sugar concentrations. Although preparation and sample handling slowed the drying process considerably, drying could not be precluded entirely. In a three hour session, mass loss was on average 0.07 g per sample (approximately 0.6% of total mass). By the conclusion of this study, samples spent between 10 to 20 hours out of the freezer so total mass loss was significant.

As wood dries, water is removed from the largest pores first, and only after the large pores are completely emptied will water begin leaving the smaller pores (Gezici-Koç, 2017; Lamason, 2015). Independent sugar measurement was only possible when the samples were initially collected so as the twigs dried the concentration of sucrose would have increased. In order to mitigate this effect, individual samples were only used 4 to 6 times so that their relative sugar concentrations would not be greatly effected.

The consequence of only using each sample a limited number of times was that not every sample could be used at both magnetic field strengths explored.

Values for diffusion are presented as the ratio of the actual diffusion coefficient for sap within the large pore structure (D) to that of free water calculated (Holtz, 2000) at the temperature of experimentation (D_0). In this way, samples measured at different lab temperatures can be compared directly.

Table 3.1 — Summary of samples used at each field strength with relevant MR properties and their sucrose concentration measured with a refractometer

Sample	Sucrose	20 MHz		1.7 MHz	
		T_{2app} (TE = 2 ms)	D/D_0	T_{2app} (TE = 3.5 ms)	D/D_0
A	1.5%	24	0.63	28	0.67
B	1.9%			30	0.70
C	1.9%	31	0.57		
D	2.3%	16	1.61		
E	2.4%	27	0.89	30	0.73
F	2.7%	32	0.56	28	0.67
G	3.0%	19	2.11	20	0.98
H	3.5%	20	0.89	15	1.44
I	3.8%	16	1.61	12	—

3.6 Discussion

Short Lifetime Signal Suppression

Within woody structures, sap vessels (large pores) are the last to fill with water and the first to empty (Lamason, 2015). As such, there will always be considerable water in the small pores whenever the large pores are able to be probed by magnetic resonance. Because diffusion in the small pores is restricted by the pore walls, diffusion information related to sucrose concentration is only accessible within the vessel water. Careful consideration must be given to address the question of how best to isolate the desired signal.

Since the signal lifetimes of the short and long lifetime components are sufficiently different (roughly one order of magnitude), they are readily separable in post-processing. At TEs similar to the short component of the T_{2app} often fewer than five data points are detectable before the short lifetime signal is entirely decayed, which makes the result of any fitting algorithm suspect. A relatively small change in the fit of the short component works a significant change in the supposed long component lifetime leading to large imprecisions in the overall measurement.

Experimental methods for isolating the signal of the large pores were explored. Signal suppression using a T_1 preparation known as STIR (Bydder and Young, 1985) was employed. This technique exploits species or water environments within a single sample that have grossly different T_1 lifetimes. The greater the difference the more effective STIR becomes. At the higher field strengths used in this study, the STIR method showed some promise, but as we moved to lower field, the T_1 lifetimes of the two signals were too similar for STIR to be effective at separating them.

At the lower field strength, the short signal had T_{2app}s in the 2 to 3 ms range. By setting the shortest TE to 2.5 ms, almost all the short signal decayed before acquisition began. Figure 3.2 shows how the first echo of the CPMG data falls above the fit line when the log of the data is plotted, demonstrating that it belongs to the short component signal. This point was omitted and fitting was completed for the single, long lifetime component signal. This procedure was both experimentally simple to implement and streamlined the data processing needed to calculate one apparent diffusion coefficient from each CPMG data set.

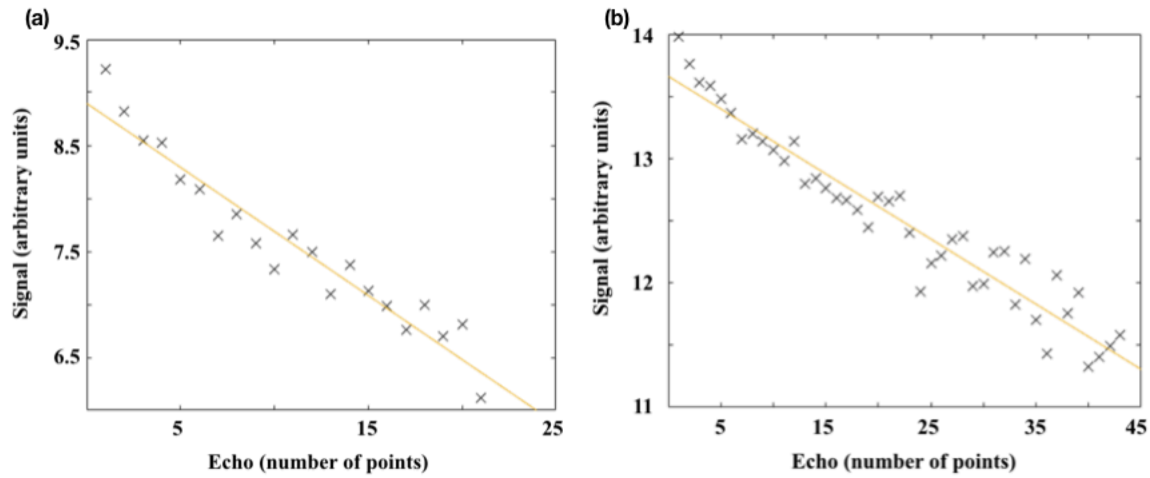

Fig. 3.2 Plot of the log of signal amplitude for sample G showing first data point(s) above the best fit line indicating that it corresponds to a pool of water with a much shorter T_{2app}. (a) CPMG measurement at 1.7 MHz with TE = 3.5 ms. (b) CPMG measurement at 20 MHz with TE = 1.5 ms. Due to an order of magnitude SNR improvement at higher field, the short lifetime component to the MR signal is more easily distinguished and characterized.

<u>20 MHz Measurements</u>

At a magnetic field of 20 MHz and an effective gradient of 57 G/cm, we would expect the sensor to have a useful sensitivity to diffusion. The data revealed a splitting of samples with five of the eight showing physically sensible, yet statistically indistinguishable, diffusion coefficients while the remaining three had diffusion coefficients that could not be physical ($D/D_0 > 1$) (Figure 3.3a). Bulky sucrose molecules should hinder the Brownian motion of the water molecules, thereby reducing the diffusion rate and this effect becomes more pronounced as sucrose concentration increases (Gill and Newling, 2022) with the physical restriction from the wood structure further reducing the apparent diffusion coefficient relative to that of free water (Callaghan, 2011).

The actual physical quantity being measured in these experiments is the MR signal lifetime, which is subsequently interpreted using the physical models above as a diffusion coefficient. When a sample appears to have a non-physical diffusion coefficient, there must be a mechanism of signal attenuation not accounted for in our model. The presence of neighbouring regions of material within a sample with differing magnetic susceptibilities will cause internal magnetic field gradients, which in turn results in additional signal attenuation. It should be noted that the samples listed in Table 3.1 that have a non-physically high diffusion coefficient are all characterized by a T_2 less than 20 ms.

We have identified two possible conditions that could produce a magnetic susceptibility within the woody structure and also a depression of the measured T_2: variations in the chemical composition of sap from tree to tree; and drying. With the current samples under investigation, we were unable to collect the ancillary data to distinguish between these two possibilities.

Within pure maple sap, a decrease in MR signal lifetime can readily be associated with an increase in the concentration of paramagnetic ions, primarily manganese (Gill and Newling, 2022). Unfortunately the volume of sap extruded from the woody samples in this study was insufficient to perform an independent chemical analysis. In an ionic solution, ions will adsorb onto the cellulose walls, which can create a large difference in magnetic susceptibility at the walls, thereby producing additional magnetic field gradients internal to the woody structure.

Large magnetic susceptibility differences can also occur at the interface between fluids (e.g. water and vapour) meaning that any pore space that is only partially filled with sap will worsen these unwanted effects. Since our measurement of diffusion requires a well defined and known magnetic gradient, these perturbations can cause apparent values of diffusion that cannot be physically real.

These effects are: well documented in rocks, trees, and other biological samples (Callaghan, 1991; Chen et al., 2005; Mitchell, 2017); much more pronounced when the direction of the magnetic field is perpendicular to the porous structure of wood (the alignment necessitated by the sensors used in the current study) due to the magnetic flux passing through regions of different magnetic susceptibility (Terenzi et al., 2013); and proportional to the magnitude of the magnetic field.

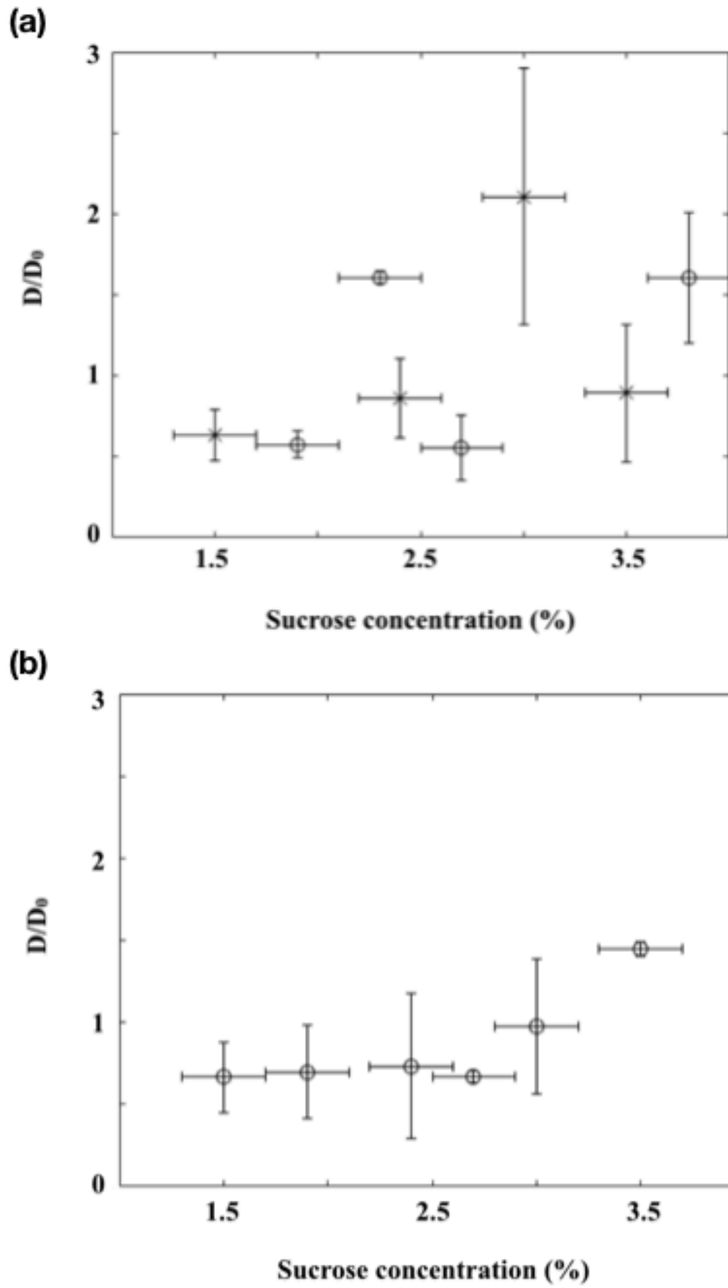

Fig. 3.3 Plots of the ratio of measured diffusion in large pore tree sap to free diffusion in water versus sugar concentration measured at time of harvest. Vertical error bars for points marked by o are the range of two measurements while for those marked with an x represent the standard deviation of four repeated measurements. (a) Diffusion measurements taken at 20 MHz. (b) Diffusion measurements taken at 1.7 MHz.

1.7 MHz Diffusion Measurements

To test whether the unexpected diffusion behaviour witnessed in Figure 3.3a was driven by magnetic susceptibility differences within our samples, we conducted a second set of measurements at the much lower field of 1.7 MHz. Of the five samples tested at lower field that had a diffusion ratio less than one, the ratios of four agreed with the values measured at 20 MHz. Sample G, which had the largest ratio at 20 MHz of 2.11, had a physically sensible diffusion coefficient when measured at 1.7 MHz (Figure 3.3b).

The final sample tested at 1.7 MHz, H, appears to have an increase in diffusion coefficient over free water, however, caution needs to be exercised. This sample experienced more drying than the others due to some damage to the epoxy. The consequence of additional drying is a reduction in diffusion sensitivity through loss of overall signal and a reduction in bulk T_2, which causes the first term in equation 3.3 to dominate the diffusion term.

Sample I had an very short T_{2app} causing lower field diffusion measurements to be unsuccessful while sample D was destroyed at an earlier stage of the study.

Considerations for Future Sensors

As mentioned above, the orientation of the cells with respect to the magnetic field plays a large role in the magnitude of susceptibility issues. These measurements could be performed at a higher field if that field were oriented along the length of the tree sample. However, a feature of this class of permanent, portable, enclosed sensors is that the field runs perpendicular to the surface (Figure 3.4). While this orientation enhances susceptibility problems, it also yields a large sensitive volume and more design control over field and gradient strengths (Marble et al., 2007) so ultimately it is an advantageous design choice. However, it may yet be beneficial to explore using portable, single-sided MR sensors.

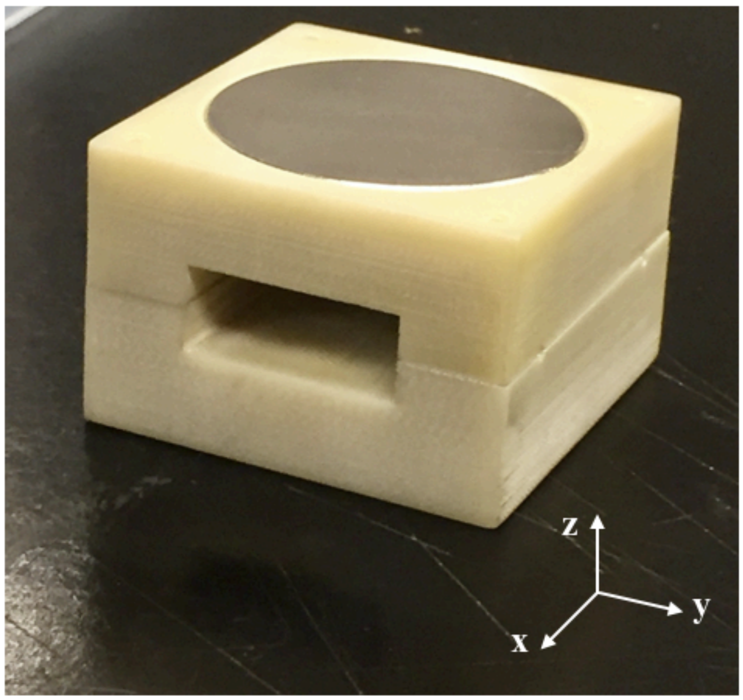

Fig. 3.4 — Photo of a 20 MHz Proteus with coordinate axes superimposed. The static magnetic field is z directed.

Based on typical MR sensors for porous rock measurements, we recommend that subsequent studies attempting to measure diffusion rates of sap within wood structure operate at 2.3 MHz (Hürlimann and Heaton, 2016; Wilson and Hürlimann, 2006), which offers a balance between signal strength and minimizing internal field changes caused by susceptibility mismatches within the sample tissue. Such a field change would account for 35% more signal than the 1.7 MHz scanner used in the current study

(Ciobanu et al., 2003; Webb and O'Reilly, 2023). It may be possible to find a compromise field strength greater than 2.3 MHz, but work would need to be done to determine at which field strength effects arising from internal susceptibility differences become problematic to diffusion measurements.

Additionally, an ideal static gradient strength would have been on the order of 100 G/cm in order to increase overall sensitivity to diffusion. Once again, there is a trade off between sensitivity to diffusion with a stronger gradient and shortening of signal lifetime due to too strong a gradient. If T_{2app} is too short, then there will not be enough breadth in the TE parameter space to probe the diffusive attenuation.

Lastly to improve the sensitivity of the rf probe, the detector coil should to be custom wound around the sample rather than having loaded the samples into a pre-formed rf probe (Windt and Blümler, 2015). Having the probe as close as possible to the sample increases overall sensitivity of the measurement. The tradeoff to this approach is the added time needed to setup the apparatus.

3.7 Conclusions

In this proof of concept study of time domain MR and diffusion measurements of maple tree cuttings, we were able to effectively separate the MR signal from three water environments: cell walls; small pores; and large pores. Two experimental and two data analysis techniques were explored to facilitate this separation. We found that signal elimination based on T_2 by careful choice of the experimental parameter TE was the simplest and most consistent approach.

Once the signal from sap in the large pores had been isolated, relative diffusion coefficients were calculated for each sample based on the attenuation of the CPMG signal as TE was varied. In the final iteration of our study performed at 1.7 MHz, we were able to reduce sample induced magnetic susceptibility differences to obtain physically sensible diffusion coefficients. These measurements were not able to show the relationship between diffusion coefficient and sap sugar concentration predicted in Gill and Newling 2022.

Experimental evidence suggests that agreement with Gill and Newling (2022) may be achievable through hardware design improvements to increase signal strength and sensitivity to diffusion as well as alternative sample handling procedures to further minimize and track radial drying and the resulting concentration changes due to moisture loss.

Chapter 4

Conclusions

4.1 MR on extruded sap

Maple sap is both a raw commodity central to the syrup industry and a natural product of the biochemical function of an individual tree. Like any biological sample, the exact chemical composition of sap varies from tree and tree and from one time to another. These natural variations depend on a host of factors including the weather period, the sap flow period, the growing conditions during the previous season, the longer term climate patterns, the overall health of the tree, and the composition of the soil, which in turn depends on the climate and on human and wildlife activity. Needless to say, these factors make a precise prediction of sap composition impossible.

As we have seen, the ^{1}H MR signal is insensitive to many of the components in tree sap due to their lack of hydrogen (e.g. minerals) or their extremely low concentration (e.g. phenolic compounds). What remains to affect the MR signal are the dissolved sugars (primarily sucrose) and naturally occurring paramagnetic and ferromagnetic ions (manganese, copper, and iron). Both of these groups reduce the relaxation time constants T_1 and T_2 proportionally to their concentrations, but the para- and ferromagnetic ions are much more efficient relaxation agents, meaning that even at small concentrations (ppm) their effect on the MR signal overshadows that of the much more abundant sugars.

However, by virtue of their small size and low concentration compared to the sugars present in sap, ferromagnetic and paramagnetic ions have little effect on the molecular self-diffusion coefficient of sap water. Instead the diffusion coefficient is determined by the concentration of dissolved sucrose in the sap. Diffusion also depends on temperature but in such a way that an experimental model can be developed to account for its effect. There are a number of methods of using magnetic resonance to measure molecular diffusion. Within the lab setting, a pulsed field gradient spin echo sequence was used to demonstrate the relationship between sucrose concentration and water diffusion coefficient.

4.2 MR on sap filled wood

Vessels within the xylem of maple wood provide a regular and predictable environment, in which to detect signal from sap. Maple trees, being diffuse-porous angiosperms, have vessels of two main sizes, and while the vessels in each category have minor variances in size, the distributions are narrow enough to be treated with discrete time constants. Water diffusion within the vessels is restricted, meaning that within the measurement time, magnetic spins come in contact with the cell walls leading to a reduction of diffusion coefficient. Because of this, only the sap within the large pores was probed in an attempt to correlate measured diffusion coefficients with the sucrose concentration of the sap.

Diffusion measurements were conducted at two field strengths, 20MHz and 1.7MHz. At the higher field, several of the samples had consistently large apparent diffusion coefficients, in fact larger than what is physically possible by a factor of 3 (see Figure 3.3). This was hypothesized to be due to sample induced magnetic field gradients caused by a magnetic susceptibility mismatch within the xylem of some of the samples. The hypothesis was tested by conducting the measurements at the lower frequency. Since the effects of magnetic susceptibility differences scale with field strength, drastically decreasing the field strength should drastically decrease the internal gradients caused by the susceptibility differences, which was confirmed in the second set of measurements.

The lower field measurements demonstrated that physically sensible diffusion coefficients for natural maple sap stored in the large xylem vessels are able to be produced by low-field MR. There was insufficient resolution in the measurements, however, to correlate diffusion to sucrose concentration of the sap due to low SNR. This issue could be overcome by using purpose built hardware in such a way as to optimize field and gradient strength while minimizing unwanted susceptibility effects. There are several approaches one could take when designing hardware specific to measuring the diffusion coefficient of sap in xylem vessels including the following sensor features: B_0 oriented along the tree stem; B_0 near 2 MHz; or a constant gradient greater than 100 G/cm.

Producing a B_0 that points along the sample with a sandwich magnetic design, the type used in this work, is not a simple task. The sensor would need to be comprised of either disk magnets with pole on the hemispheres or ring magnets to allow the sample to be fed up through their centres. The disk magnet option would suffer from an unstable orientation since like poles would need to be facing each other. On the other hand, the arrangement of the ring design would be mechanically stable, but it is questionable whether a usefully uniform field could be produced across the long gap needed to fit the MR probe. Alternatively, the sensor could be an open-faced, single sided, three magnet array design. Single sided sensors benefit from ease of loading samples and flexibility in shaping the static gradient; however these designs tend to have low field strengths around 2 to 5 MHz.

Using a field near 2 MHz is essentially a trade off between susceptibility effects and adverse SNR. As we saw in chapter 3, the measurement time to produce one diffusion coefficient was 40 to 50 minutes at 1.7 MHz and even then, the results were hampered by low SNR. It is questionable if a measurement in the field would be truly useful with such a long timescale.

SNR and measurement time were not issues at 20 MHz. Instead, those measurements suffered the most from internal field gradients, which caused over estimations of some diffusion coefficients by as much as a factor of three. This indicates that the internal field gradients were on the same order as the exterior field. Rather than dropping to a much lower field to minimize the internal gradients, we could hold the field strength at 20 MHz and increase the external gradient such that its effect dominates over the susceptibility induced gradients. This scheme would require an external gradient of at least 100 G/cm, which is readily possible by adding a pitch to the Proteus design. The unwanted consequence of increasing the gradient strength is additional diffusive attenuation in the MR signal leading to shorter apparent T_2 values. This decreases the parameter space available to probe sap diffusion and makes the analysis, including separation of short and long sap signals more difficult.

Regardless of the different approaches listed above, all of the sensor options are low cost, readily portable, handheld, (weighing much less than 1 kg), with a constant, static gradient. These features streamline the hardware involved to operate and eliminate the need for separate gradient coils, controls, and power supplies, thus making them easier to deploy in the field.

4.3 Possible applications of current work

A non-invasive measurement of sucrose concentration in a living maple treeling would be useful to industry and the research community, and the work of this thesis lays out the foundations of such a measurement. Diffusion measurements of sap filled vessels, given sufficient precision, can be used to rank young trees by their ability to produce sweet sap. Such a ranking, in turn, can be used to inform purposeful planting or thinning activities to increase the overall productivity and profitability of a sugar bush. For researchers, this would also open new possibilities for monitoring how environmental stresses and climate change affect the sucrose concentration of sap throughout the growth phase of young trees.

Even without this precision, the work of this thesis has demonstrated that low-resolution, handheld MR sensors are capable of monitoring the pore size distributions in very young trees less than 1cm in diameter. This goes beyond maple trees and is applicable to any woody plant, meaning that pore size can be monitored in-vivo without coring or sectioning the plant, giving researchers another tool in the work to understand how climate change impacts the growth of xylem vessels.

4.4 Opportunities for further study

Syrup Adulteration

Maple syrup is an iconic and valuable foodstuff and staying ahead of counterfeiters is important to safeguarding the reputation and quality of genuine product. There are several measurements currently in use for detecting if syrup has been adulterated, largely relying on various forms of spectroscopic analysis. Processing maple sap into syrup produces niter (also called sugar sand) which is a gritty mixture of organic compounds and inorganic minerals that saturate out of solution. Because of this, different batches of maple syrup tend to have more uniformity in their chemical composition than raw sap does. As such, it will have a predictable range of associated MR relaxation times.

The work in chapter two suggests that a bench top magnetic resonance measurement could also be used to assess the purity of maple syrup. These types of instruments are already deployed for quality assurance in other food production because of their relatively low-cost and turnkey setup and analysis. This measurement could also be done with a portable, single-sided MR sensor, which would have the added benefit of being able to non-invasively scan through a glass bottle. Such a measurement could become an inspection tool at a point of export to safeguard against fraudulent maple syrups leaving the country.

Sap flow monitoring without external gradients

As previously mentioned in section 1.3, both weather during the maple season and anatomical features of individual trees are important driving factors for seasonal sap flow. While there are silviculture activities, such as tree thinning, that can improve sap flow by optimizing sun in a maple stand, a tree's anatomy is fixed. I have collected some first and second hand anecdotal evidence that certain trees, which appear to be favourably positioned for sap flow amongst its neighbours, have sap that either flows poorly or not at all.[4]

MR has the ability to measure fluid flow, but this is typically done using external magnetic field gradients, which are hardware intensive. In situ sap flow has been successfully monitored by several MR research groups using such systems (see section 1.4). The types of handheld sensors used in this thesis can also be used for measuring flow speed when their constant gradients are appropriately shaped by adding a pitch between the two magnets inside the sensor (Guo et al., 2021; Morin et al., 2024). The measurement involves monitoring how the signal phase of the second echo in a CPMG sequence changes as a function of changing τ (cf. Figure 1.2). Such a measurement cannot be spatially resolved, instead it would report the average sap speed across the stem, which is still an important quantity to ascertain.

[4] Including a story from one of my uncles who cut down one particular maple tree out of spite after it failed to produce a drop of sap over years of attempted tapping.

Works Cited

Araujo CD, MacKay AL, Hailey JRT, Whittall KP, Le H (1992) Proton magnetic resonance techniques for characterization of water in wood: application to white spruce. Wood Science and Technology. https://doi.org/10.1007/BF00194466

Aroulmoji V, Mathlouthi M, Feruglio L, Murano E, Grassi M (2012) Hydration properties and proton exchange in aqueous sugar solutions studied by time domain nuclear magnetic resonance. Food Chemistry.132:1644-1655. https://doi.org/10.1016/j.foodchem.2011.01.110

Bloembergen N, Purcell EM, Pound RV (1948) Relaxation Effects in Magnetic Resonance Absorption. Physical Review 73(7).

Blümich B, Mauler J, Haber A, Perlo J, Danieli E, Casanova F (2009) Mobile NMR for geophysical analysis and materials testing. Petroleum Science. 6:1-7. https://doi.org/10.1007/s12182-009-0001-4

Boston M, Ragauskas AJ (2010) Changes in the Structure of the Cellulose Fiber Wall during Dilute Acid Pretreatment in Populus Studied by 1H and 2H NMR. Energy Fuels 24: 5677-5685.

Bydder GM, Young IR (1985) MR Imaging: Clinical use of the inversion recovery sequence. Journal of Computer Assisted Tomography 9(4):659-675

Callaghan P (1991) Principles of Nuclear Magnetic Resonance Microscopy. Oxford: Oxford University Press

Callaghan P (2011) Translational Dynamics & Magnetic Resonance. Oxford: Oxford University Press

Cao H, Lyu J, Zhou Y, Gao X (2021) The Study of Bound Water Status and Pore Size Distribution of Chinese Fir and Poplar Cell Wall by Low-Field NMR. International Journal of Polymer Science. https://doi.org/10.1155/2021/4954837

Capitani D, Sobolev AP, Di Tullio V, Mannina L, Proietti N (2017) Portable NMR in food analysis. Chemical and Biological Technologies in Agriculture. 4-17. https://doi.org/10.1186/s40538-017-0100-1

Casanova F, Perlo J (2011) NMR in Inhomogeneous Fields. In: Casanova F, Perlo J, Blümich B (eds) Single-Sided NMR. Berlin: Springer

Chen Q, Marble AE, Colpitts BG, Balcom BJ (2005) The internal magnetic field distribution, and single exponential magnetic resonance free induction decay, in rocks. Journal of Magnetic Resonance. https://doi.org/10.1016/j.jmr.2005.05.001

Ciobanu L, Webb AG, Pennington CH (2003) Magnetic resonance imaging of biological cells. Progress in Nuclear Magnetic Resonance Spectroscopy 42:69–93

Cortes PM, and TR Sinclair (1984) The Role of Osmotic Potential in Spring Sap Flow of Mature Sugar Maple Trees (Acer sacchdrum Marsh). Journal of Experimental Botany 36(162): 12-24.

Clément A, Panneton B, Martin N, Lagacé L (2014) Maple syrup quality control. Canadian Food Insights. 34-35.

Da-Yan M, Xi-Ming W, Ming-Hui Z, Xue-Qi L (2012) Quantitative separation of NMR signal amplitude of water in wood on the basis of T2. Materials Science Forum. https://doi.org/10.4028/www.scientific.net/MSF.704-705.552

Decker KLM, Wang D, Waite C, Scherbatskoy T (2003) Snow Removal and Ambient Air Temperature Effects on Forest Soil Temperatures in Northern Vermont. Soil Science Society of America Journal 67(4): 1234-1243.

De León−Rodríguez LM, Martins AF, Pinho MC, Rofsky N, Sherry AD (2015) Basic MR relaxation mechanisms and contrast agent design, Journal of Magnetic Resonance Imaging. 42:545-565.

Eisberg R, Resnick R (1985) Quantum Physics of Atoms, Molecules, Solids, Nuclei, and Particles, second edition. New York: Wiley.

Elder T, Labbé N, Harper D, Rials T (2006) Time domain-nuclear magnetic resonance study of chars from souther hardwoods. Biomass and Bioenergy 30: 855-862.

Eustace CA, Jordan RB (1995) Sugar content evaluation using Earth's field proton magnetic resonance. American Society of Agricultural Engineers. 38.5:1563-1571.

Fabri D, Williams MAK, Halstead TK (2005) Water T2 relaxation in sugar solutions. Carbohydrate Research. 340:889-905. https://doi.org/10.1016/j.carres.2005.01.034

Gao X, Zhuang S, Jin J, Cao P (2015) Bound Water Content and Pore Size Distribution in Swollen Cell Walls Determined by NMR Technology. BioResources 10(4): 8208-8224.

Gezici-Koç Ö, Erich SJF, Huinink HP, van der Ven LGJ, Adan OCG (2017) Bound and free water distribution in wood during water uptake and drying as measured by 1D magnetic resonance imaging. Cellulose. https://doi.org/10.1007/s10570-016-1173-x

Griffith DJ (2017) Introduction to Electrodynamics, fourth edition. Cambridge: Cambridge University Press.

Gill M, Newling B (2022) The Determination of Sucrose Content in Maple Sap Using Time-Domain Magnetic Resonance. Sugar Tech 24 882-889

Government of Canada (2020) Statistical Overview of the Maple Industry 2019. https://multimedia.agr.gc.ca/pack/pdf/maple_erable_2019a-eng.pdf. Accessed 15 April 2021.

Graf I, Ceseri M, Stockie JM (2015) Multiscale model of a freeze –thaw process for tree sap exudation. Journal of the Royal Society Interface 12: 20150665 http://dx.doi.org/10.1098/rsif.2015.0665

Guo J, Ross MMB, Newling B, Lawrence M, Balcom BJ (2021) Laminar flow characterization using low-field magnetic resonance techniques. Physics of Fluids 33, 103609 doi: 10.1063/5.0065986

Harrison JL, Reinmann AB, Maloney AS, Phillips N, Juice SM, Webster AJ, Templer PH (2020) Transpiration of Dominant Tree Species Varies in Response to Projected Changes in Climate: Implications for Composition and Water Balance of Temperate Forest Ecosystems. Ecosystems 23: 1598-1613.

Holz M, Heil SR, Sacco A (2000) Temperature-dependent self-diffusion coefficients of water and six selected molecular liquids for calibration in accurate 1H NMR PFG measurements. Physical Chemistry Chemical Physics. 2:4740-4742. https://doi.org/10.1039/B005319H

Hürlimann MD, Heaton NJ (2016) NMR Well Logging. In: Johns M, Fridjonsson E, Vogt S, and Haber A (eds) Mobile NMR and MRI: developments and applications. Cambridge: The Royal Society of Chemistry, pp 11-85

Ishikawa M, Ide H, Price WS, Arata Y, Nakamura T, Kishimoto T (2009) Freezing behaviours in plant tissues: visualization using NMR micro-imaging and biochemical regulatory factors involved. In: Gusta L, Wisniewski M, Tanino K (eds) Plant cold hardiness: from the laboratory to the field. CABI pp 19-28

Lamason C, MacMillan B, Balcom BJ, Leblon B, Pirouz Z (2015) Water content measurement in black spruce and aspen sapwood with benchtop and portable magnetic resonance devices. Wood Material Science & Engineering. http://dx.doi.org/10.1080/17480272.2015.1010573

Lamason C, MacMillan B, Balcom BJ, Leblon B, Pirouz Z (2017) Magnetic resonance studies of wood log-drying processes. Forest Products Journal 67(3/4): 266-274

Lagacé L, Leclerc S, Charron C, Sadiki M (2015) Biochemical composition of maple sap and relations among constituents. Journal of Food Composition and Analysis. 41:129-136. https://doi.org/10.1016/j.jfca.2014.12.030

Malone MW (2016) In vivo Observation of Tree Drought Response with Low-Field NMR and Neutron Imaging. Frontiers in Plant Science. doi.org/10.3389/fpls.2016.00564.

Marble AE, Mastikhin IV, Colpitts BG, Balcom BJ (2007) A compact permanent magnet array with a remote homogenous field. Journal of Magnetic Resonance 186: 100-104

Meixner M, Kochs J, Foerst P, Windt CW (2021) An integrated magnetic resonance plant imager for mobile use in greenhouse and field. Journal of Magnetic Resonance. doi.org/10.1016/j.jmr.2020.106879.

Menon RS, MacKay AL, Halley JRT, Bloom M, Burgess AE, Swanson JS (1987) An NMR determination of the physiological water distribution in wood during drying. Journal of Applied Polymer Science 33:1146-1155.

Morin DM, Richard S, Asnaribaranghar N, Newling B, Balcom BJ (2024) A low-field ceramic magnet design for magnetic resonance. Journal of Magnetic Resonance. https://doi.org/10.1016/j.jmr.2023.107599

Mitchell J (2017) Industrial applications of magnetic resonance diffusion and relaxation time measurements. In: Valiullin R (ed) Diffusion NMR of confined systems: fluid transport in porous solids and heterogeneous materials. London: The Royal Society of Chemistry, pp 353-389

Nagata A, Kose K, Terada Y (2016) Development of an outdoor MRI system for measuring flow in a living tree. Journal of Magnetic Resonance. http://dx.doi.org/10.1016/j.jmr.2016.02.004.

Nishimura DG (2010) Principles of Magnetic Resonance Imaging. Self published: lulu.com.

Pallardy SG (2008) Physiology of Woody Plants Third Edition. Academic Press.

Parigi G, Luchinat C (2018) NMR Consequences of the Nucleus-Electron Spin Interactions. In Paramagnetism in Experimental Biomolecular NMR, eds. Luchinat C, Parigi G, Ravera E, 1-41. London: Royal Society of Chemistry.

Pelletier DB (2023) Maple Syrup Under Threat. Radio-Canada. https://ici.radio-canada.ca/info/2023/sirop-erable-rechauffement-climat-niche-production-acericole-cabane-sucre-printemps-seve-quebec/en/. Accessed 7 July 2023

Perkins TD, van den Berg AK (2009) Maple syrup-production, composition, chemistry, and sensory characteristics. Advances in Food and Nutrition Research 56:101-143.

Rademacher T, Cliche M, Bouchard E, Kurokawa SYS, Rapp J, Deslauriers A, Messier C, Rossi S, Dupras J, Filotas E, Delagrange S (2023) TAMM review: On the importance of tap and tree characteristics in maple sugaring. Forest Ecology and Management 535, 120896 https://doi.org/10.1016/j.foreco.2023.120896.

Robitaille G, Boutin R, Lachance D (1995) Effects of soil freezing stress on sap flow and sugar content of mature sugar maples (Acer saccharum). Canadian Journal of Forestry Research 25: 577-587.

Ross MMB, Wilbur GR, Cano Barrita PFdJ, Balcom BJ (2021) A portable, submersible, MR sensor – The Proteus magnet, Journal of Magnetic Resonance. 326:1-8. https://doi.org/10.1016/j.jmr.2021.106964

Selby W, Balcom BJ, Newling B, Mastikhin I (2024) Using phase interference to characterize dynamic properties — a review of constant gradient, portable magnetic resonance methods. Frontiers in Physics 11:1201032 doi: 10.3389/fphys.2023.1201032

Sorin C, Mariette F, Musse M, Leport L, Cruz F, Yvin JC (2018) Leaf Development Monitoring and Early Detection of Water Deficiency by Low Field Nuclear Magnetic Resonance Relaxation in Nicotiana tabacum Plants. Applied Science. doi:10.3390/app8060943

Staats LJ (1992) Progeny testing 10-year old sugar maple families for sugar sap concentration. M.Sc. thesis. State University of New York.

Stait-Gardner T, Kumar PGA, Price WS (2008) Steady state effects in PGSE NMR diffusion experiments, Chemical Physics Letters. 462:331-336. https://doi.org/10.1016/j.cplett.2008.07.084

Taylor FH (1956) Variation in sugar content of maple sap. Vermont Agricultural Experiment Station Bulletin. 587:3-39.

Terada Y, Horikawa Y, Nagata A, Kose K, Fukuda K (2019) Dynamics of xylem and phloem sap flow in an outdoor zelkova tree visualized by magnetic resonance imaging. Tree Physiology. doi:10.1093/treephys/tpz120.

Terenzi C, Dvinskikh SV, Furó I (2013) Wood microstructure explored by anisotropic 1H-NMR line broadening: experiments and numerical simulations. The Journal of Physical Chemistry B. https://dx.doi.org/10.1021/jp4043733

Tyree MT (1983) Maple sap uptake, exudation and pressure changes correlated with freezing exotherms and thawing endotherms. Plant Physiology 73: 277-285.

Weaver NJ, Wilkin GS, Morison KR, Watson MJ (2020) Minimizing the energy requirements for the production of maple syrup. Journal of Food Engineering. https://doi.org/10.1016/j.jfoodeng.2019.109823

Webb A, O’Reilly T (2023) Tackling SNR at low−feld: a review of hardware approaches for point−of−care systems. Magnetic Resonance Materials in Physics, Biology and Medicine. https://doi.org/10.1007/s10334-023-01100-3

Wild AD, Yanai RD (2015) Soil nutrients affect sweetness of sugar maple sap. Forest Ecology and Management 341: 30-36.

Wilson RC, Hürlimann MD (2006) Relationship between susceptibility induced field inhomogeneities, restricted diffusion, and relaxation in sedimentary rocks. Journal of Magnetic Resonance. https:/doi.org/10.1016/j.jmr.2006.07.006

Windt, CW, Blümler P (2015) A portable NMR sensor to measure dynamic changes in the amount of water in living stems or fruit and its potential to measure sap flow. Tree Physiology. 35, 366-375. https://doi.org/10.1093/treephys/tpu105

Windt CW, Nabel M, Kochs J, Jahnke S, Schurr U (2021) A Mobile NMR Sensor and Relaxometric Method to Non-destructively Monitor Water and Dry Matter Content in Plants. Frontiers in Plant Science. doi.org/10.3389/fpls.2021.617768.

Xin G, Zhuang S, Jin J, Cao P (2015) Bound water content and pore size distribution in swollen cell walls determined by NMR technology. BioResources. https://doi.org/10.15376/biores.10.4.8208-8224

Ziegler GR, MacMillan B, Balcom BJ (2003) Moisture migration in starch molding operations as observed by magnetic resonance imaging. Food Research International. 36:331-340. https://doi.org/10.1016/S0963-9969(02)00224-7

Zimmermann MH, Brown CL (1971) Trees: Structure and Function. Springer-Verlag.

Curriculum Vitae

Michael Gill

Acadia University, Master of Arts in Theology, 2010
University of New Brunswick, Bachelor of Science in Physics, 2007

Publications:

Michael Gill and Benedict Newling, The determination of sucrose content in maple sap using time-domain magnetic resonance, *Sugar Tech* (2022) 24, 882-889.

Michael E. Gill, *Studies on the translator of 1 Esdras with a particular interest in the work of Zipora Talshir* (2010) MA thesis, Acadia University.

Conference Presentations:

Michael Gill, “The textual development of the Greek book 1 Esdras” (2011) Canadian Society of Biblical Studies.

Michael Gill, “Avoiding misunderstandings in the classroom pertaining to science and religion” (2007) Atlantic Canadian Association of Science Educators.

Michael Gill, "The Propagation of Electromagnetic Disturbances in the Earth's Plasma Sheet” (2006) Canadian Undergraduate Physics Conference.

Michael Gill, “Methodology of teaching field theory at a high school level” (2005) Atlantic Canadian Association of Science Educators.